

# 1 The Late Quaternary tephrostratigraphy of annually laminated sediments from 2 Meerfelder Maar, Germany

3 Christine S. Lane<sup>1,2,\*</sup>, Achim Brauer<sup>3</sup>, Celia Martín-Puertas<sup>3</sup>, Simon P.E. Blockley<sup>4</sup>, Victoria C.  
4 Smith<sup>2</sup> and Emma L. Tomlinson<sup>5,6</sup>.

5 <sup>1</sup> Department of Geography, University of Manchester, Arthur Lewis Building, Oxford Road, Manchester, M13  
6 9PL, United Kingdom.

7 <sup>2</sup> Research Laboratory for Archaeology and the History of Art, University of Oxford, Dyson Perrins Building,  
8 South Parks Road, Oxford, OX1 3QY, United Kingdom.

9 <sup>3</sup> GFZ German Research Centre for Geosciences, Section 5.2 Climate Dynamics and Landscape Evolution,  
10 Potsdam, Germany.

11 <sup>4</sup> Centre for Quaternary Research, Royal Holloway University of London, Egham, Surrey, TW20 0EX, United  
12 Kingdom.

13 <sup>5</sup> Department of Geology, Trinity College Dublin, College Green, Dublin 2, Republic of Ireland.

14 <sup>6</sup> Department of Earth Sciences, Royal Holloway University of London, United Kingdom.

15 \*corresponding author: [christine.lane@manchester.ac.uk](mailto:christine.lane@manchester.ac.uk)

16

## 17 Abstract

18 The record of Late Quaternary environmental change within the sediments of Meerfelder  
19 Maar in the Eifel region of Germany is renowned for its high precision chronology, which is  
20 annually laminated throughout the Last Glacial to Interglacial transition (LGIT) and most of  
21 the Holocene. Two visible tephra layers are prominent within the floating varve chronology  
22 of Meerfelder Maar. An Early Holocene tephra layer, the Ulmener Maar Tephra (~11,000  
23 varve years BP), provides a tie-line of the Meerfelder Maar record to the varved Holocene  
24 record of nearby Lake Holzmaar. The Laacher See Tephra provides another prominent time  
25 marker for the late Allerød, ~200 varve years before the transition into the Younger Dryas at  
26 12,680 varve years BP. Further investigation has now shown that there are also 15  
27 cryptotephra layers within the Meerfelder Maar LGIT-Holocene stratigraphy and these  
28 layers hold the potential to make direct comparisons between the Meerfelder Maar record  
29 and other palaeoenvironmental archives from across Europe and the North Atlantic. Most  
30 notable is the presence of the Vedde Ash, the most widespread Icelandic eruption known  
31 from the Late Quaternary, which occurred midway through the Younger Dryas. The Vedde  
32 Ash has also been found in the Greenland ice cores and can be used as an isochron around  
33 which the GICC05 and Meerfelder Maar annual chronologies can be compared. Near the  
34 base of the annual laminations in Meerfelder Maar a cryptotephra is found that correlates  
35 to the Neapolitan Yellow Tuff, erupted from Campi Flegrei in southern Italy, 1200 km away.  
36 This is the furthest north that the Neapolitan Yellow Tuff has been found, highlighting its  
37 importance in the construction of a European-wide tephrostratigraphic framework. The co-  
38 location of cryptotephra layers from Italian, Icelandic and Eifel volcanic sources, within such  
39 a precise chronological record, makes Meerfelder Maar one of the most important  
40 tephrostratotype records for continental Europe during the Last Glacial to Interglacial  
41 transition.

42 **Keywords:** tephrostratigraphy, cryptotephra, Lateglacial, varves, Meerfelder Maar.

43

## 44 1. Introduction

45 The detection of microscopic layers of volcanic ash (cryptotephra) within terrestrial, marine  
46 and ice core records is revolutionising the way widespread palaeoenvironmental archives  
47 are dated and compared. Tephra isochrons provide stratigraphic tie-lines between records,  
48 which permit precise inter-site correlation and comparison of the proxy record, whilst

49 avoiding un-grounded assumptions of synchronicity. In addition, where tephra can be  
50 correlated to eruptions of known age, absolute age estimates can be achieved and  
51 transferred between records. Consequently, the last two decades have seen rapid growth in  
52 cryptotephra research, most notably within Late Quaternary palaeoenvironmental studies  
53 (e.g., Dugmore et al., 1995; Lowe, 2001; Wulf et al., 2004), but also within archaeological  
54 investigations (e.g., Plunkett, 2009; Housley et al., 2012; Lane et al., 2014). Across Europe in  
55 particular, there is now a wealth of tephrostratigraphic and chronological data that can be  
56 built into a regional tephrostratigraphic framework of interconnected sites, within which  
57 questions about the timing of environmental and climatic changes can be addressed  
58 (Blockley et al., 2012; Davies et al., 2012; Lane et al., 2012a; Wulf et al., 2013).

59 Key to the development of a regional tephrostratigraphic framework are two different sorts  
60 of distal sites: (i) *linking sites* that contain tephra records of multiple eruptions from  
61 different volcanic sources (e.g., Lane et al., 2011a) and (ii) *chronological reference sites* with  
62 annual to decadal precision, that can feedback dating information to sites around the  
63 network (e.g. the Greenland ice core records, Mortensen et al., 2005; Abbott and Davies,  
64 2012). The rare sites that are able to fulfil both of these criteria are typically (partially, or  
65 wholly) varved records that sit within the fallout ranges of multiple volcanic centres.  
66 European examples include the Lateglacial to Early Holocene record in Soppensee,  
67 Switzerland (Hajdas, 1993; Lane et al., 2011b) and the 133 ka record in Lago Grande di  
68 Monticchio, Italy (Wulf et al., 2004; Wulf et al., 2008; Wulf et al., 2012).

69 A major strength of varve sequences lies in the opportunity to date the intervals between  
70 tephra isochrons, with annual to decadal precision. This *differential dating* approach  
71 provides important chronological constraints that can be built into a regional  
72 tephrostratigraphic framework and used to precisely compare periods of known equivalent  
73 duration wherever the same tephra layers are found co-registered. The combination of  
74 widespread tephra layers in varve palaeoenvironmental sequences therefore provides the  
75 rare, but exceptionally valuable, opportunity to study subtle variations in the timing and  
76 rate of environmental response to past abrupt climate changes (Lane et al., 2013).

77 A cryptotephra study of the Lateglacial to Holocene age sediments from Meerfelder Maar,  
78 in the Eifel region of Germany, was carried out with the aim of establishing a new European  
79 tephrostratotype sequence in a site that has high (seasonal to annual) chronological  
80 resolution as well as the potential to contain tephra from a number of European volcanic  
81 centres (the Eifel, Massif Central, Icelandic and Italian). This paper presents the full results  
82 of this study, with the following three objectives:

- 83 i. To report the Lateglacial and Holocene tephrostratigraphy of Meerfelder Maar.
- 84 ii. To provide improved varve-age estimates, with uncertainties, for a number of the tephra  
85 layers within Meerfelder Maar and to constrain the inter-eruption ages.
- 86 iii. To place the Meerfelder Maar record within a broader European tephrostratigraphic  
87 framework, which permits direct correlation of palaeoenvironmental archives from the  
88 North Atlantic, Europe and the Mediterranean.

89

## 90 2. Site & methods

### 91 2.1. The site

92 Lake Meerfelder Maar (50°06' N, 6 ° 45' E, 336.5 m a.s.l.) is located in the Eifel region,  
93 Germany (Fig. 1), within a volcanic crater formed a minimum of 30 ka BP according to  
94 previous radiocarbon dating (Büchel and Lorenz, 1984; Brauer et al., 1999) or even ca 80 ± 8

95 ka BP according to recent thermoluminescence dating (Zöller and Blanchard, 2009). The lake  
96 has a surface area of approximately 248 m<sup>2</sup> and a maximum depth of 18 m. The lake  
97 catchment is small, defined by the steep, vegetated, crater walls, which reach up to 520 m  
98 at their highest.

99 The Holocene varved sediments are composed of spring/summer diatomaceous organic  
100 sub-layers and winter sub-layers of allochthonous sediment (Brauer et al., 1999), whereas  
101 the lateglacial sediments exhibit a succession of different varves types including siderite  
102 varves (late Allerød) and clastic-dominated snow melt varves (second half of Younger  
103 Dryas), triggered by rapid climate changes and lake evolution (Brauer et al., 1999). The  
104 sediment formation in Lake Meerfelder Maar is sensitive to North Atlantic climate  
105 variability. Abrupt sedimentary and biological responses to Lateglacial and Holocene climatic  
106 shifts recorded at Meerfelder have provided new insights into the nature and mechanism of  
107 Late Quaternary climate dynamics (Brauer et al., 2008; Martin-Puertas et al., 2012a; Martin-  
108 Puertas et al., 2012b; Lane et al., 2013).

## 109 2.2. Field work and varve counting

110 During a coring expedition in 2009 seven new and parallel core sequences were retrieved  
111 from the deepest part of the lake basin using a UWITEC piston corer. The maximum distance  
112 between individual coring sites was 20 m. These sediment profiles, labelled as cores  
113 MFM09-A to MFM09-G, were split, imaged, described and correlated. Each of this sediment  
114 profiles consists of a sequence of 5-6 up to 2 m long core segments, typically with gaps of a  
115 few cm between each individual core. Two sediment profiles were selected for thin sections  
116 analyses: core MFM09-A (11.50 m long) and core MFM09-D (10.58 m long). Core A was  
117 recovered from the water/sediment interface, whereas core D starts 70 cm below. A  
118 composite profile (MFM09; 11.71 m long) was constructed through detailed correlation  
119 based on macroscopic and microscopic marker layers. Martin-Puertas et al. (2012) used the  
120 same marker layers to correlate the new sediment profile with a previous profile MFM-6  
121 (Brauer et al., 1999; Brauer et al., 2000a). The new continuous sediment record (MFM09) so  
122 far has been investigated in particular for Holocene climate and environment changes  
123 (Martin-Puertas et al., 2012a).

124 Varve counting was carried out on a continuous series of thin sections (100 x 35 mm, with 2  
125 cm overlaps) using a petrographic microscope under parallel and polarized light (Brauer et  
126 al., 1999; Martin-Puertas et al., 2012a). Varve counting involved thickness measurements  
127 for each varve at higher microscopic magnification (100x). In order to assess the individual  
128 error, varve counting was realized twice by the same counter.

## 129 2.3. Cryptotephra investigations

130 The entire core sequence MFM09-D was investigated for the presence of cryptotephra  
131 following the non-destructive density floatation method of Turney (1998); Blockley et al.  
132 (2005). Tephra glass shards within the 1.95-2.55 g/cm<sup>3</sup> residue (and also >2.55 g/cm<sup>3</sup> for low  
133 resolution samples) were identified and absolute numbers counted under high powered  
134 polarised light microscopy, then quantified as shards per gram of dry sediment (s/g). Where  
135 tephra glass shards were discovered in initial low-resolution contiguous samples, these 10  
136 cm lengths were re-investigated at 1 cm resolution to better define the location of the  
137 tephra layer. Where possible, thin section inspection of the cores was then used to locate  
138 the tephra layer to its exact varve position. All Tephra layers are given sample codes based

139 upon their first occurrence depth below lake floor (cm) and these are used throughout the  
140 manuscript.

#### 141 2.4. Geochemical analysis

142 In order to concentrate glass shards for geochemical analysis, they were picked from  
143 samples under high-powered microscopy, using a gas chromatography syringe (Lane et al.,  
144 2014). The tephra shards were then mounted in epoxy resin, sectioned and polished for  
145 geochemical analysis. Major and minor element concentrations were measured by  
146 wavelength dispersive electron probe micro-analysis (WDS-EMPA), using the Jeol JXA 8600  
147 microprobe in the Research Laboratory for Archaeology, University of Oxford. Instrument  
148 operating conditions: 15 keV accelerating voltage, 6 nA current, 10  $\mu\text{m}$  beam diameter and  
149 10–30 s peak count times. The ATHO-g (rhyolitic) and StHs6/80-g (andesitic) MPI-DING fused  
150 volcanic glass secondary standards (Jochum et al., 2006) were analysed with the tephra  
151 samples to monitor instrument precision and accuracy (Supplementary Information Table  
152 S2). Major element ( $\text{SiO}_2$ ,  $\text{Al}_2\text{O}_3$ ,  $\text{FeO}_{\text{tot}}$ ,  $\text{CaO}$ ,  $\text{Na}_2\text{O}$ ,  $\text{K}_2\text{O}$ ) precision on secondary standard  
153 analyses ranges from  $<1$  to  $<10$  % (at  $2\sigma$ ), precision for the less abundant elements varies  
154 between 10-30%.

155 Trace element compositions were measured by laser ablation inductively coupled plasma  
156 mass spectrometry (LA-ICP-MS), using the Agilent 7500 ICP-MS coupled to a 193 nm  
157 Resonetics ArF eximer laser ablation system, in the Department of Earth Sciences, Royal  
158 Holloway University of London. Analytical protocols and data quantification followed those  
159 described in Tomlinson et al. (2010): a 5Hz repetition rate and 40 second sample and gas  
160 blank count times were used. NIST 612 was used as a standard for calibration, with  $^{29}\text{Si}$  as  
161 the internal standard element having been previously measured by WDS-EPMA within each  
162 individual grain. Laser spot sizes of between 25  $\mu\text{m}$  and 34  $\mu\text{m}$  were used according to the  
163 size of the glass shards. For consistency with WDS-EMPA, the ATHO-g and StHs6/80-g MPI-  
164 DING secondary glass standards were used to monitor precision and accuracy  
165 (Supplementary Information Table S2). Precision on secondary standard analyses (at  $2\sigma$ )  
166 averages  $< 10$  % for all elements, with the exception of Sm, Dy and Yb,  $<18\%$ , which are  
167 present in very low concentrations. Due to small grain sizes and low glass shard  
168 concentrations (section 3.1), not all samples were successfully analysed by LA-ICP-MS.

### 169 3. Results

170 The uppermost two meters of the new core MFM09 are not laminated, but varves are well-  
171 preserved over most of the lower part of the record. This confirms reports from the  
172 previous MFM-6 core (Brauer et al., 2000).

#### 173 3.1. Varve chronology

174 In this study, we present a new and slightly revised varve chronology for MFM labelled as  
175 MFM2015 chronology. This chronology has been established for the latest MFM composite  
176 profile (MFM-09) and is for the Holocene part (0-753 cm sediment depth) identical with the  
177 MFM2012 chronology (Martin-Puertas et al. (2012a). For the interval from the Laacher See  
178 Tephra (LST; 12,880 varve yrs BP, late Allerød) up to the early Holocene Ulmener Maar  
179 tephra (UMT; 11,000 varve yrs BP) the chronology is identical to the MFM-6 chronology  
180 (Brauer et al., 1999). Varve ages were transferred from the MFM-6 to the MFM-09 core  
181 sequence (753-876 cm depth interval) through correlating a series of macroscopic and  
182 microscopic marker layers. The revision only affects the older part of the lateglacial

183 sediment interval below the LST down to the onset of distinct and continuous varve  
184 preservation (876-1073 cm sediment depth, Fig. 2-3). Because of the better varve  
185 preservation in this section of the new composite MFM-09 profile this interval has been re-  
186 counted and revealed in total  $1350 \pm 50$  varves, i.e. 100 varves more than in the previous  
187 MFM-6 chronology (Fig. 3). This resulted in a revised age for the onset of continuous varve  
188 preservation at  $14,230 \pm 90$  varve yrs BP. Absent or very poor varve preservation prevented  
189 from varve counting in the early Lateglacial interstadial. The duration of ca. 400 years from  
190 the beginning of the Lateglacial interstadial, defined as Meiendorf pollen zone by Litt and  
191 Stebich (1999), thus had to be extrapolated based on measured varve thickness in the  
192 lowermost interval of continuous varve occurrence (Fig. 3).

193 The error estimate for the new MFM2015 chronology adds  $\pm 50$  varve yrs derived from  
194 multiple counting of the revised section to the previously defined error estimate for the LST  
195 ( $12,880 \pm 40$  varve yrs BP; Lane et al., 2013). The resulting error estimate for the age of the  
196 onset of continuous varve formation in MFM ( $14,230 \pm 90$  varve yrs BP) is considered a  
197 minimum error because the counted interval includes a small slumped section which is also  
198 present in the MFM-6 sediment profile (Brauer et al., 2000b). The duration of this section  
199 (110 estimated varve years) has been calculated by interpolation and adopted from the  
200 MFM-6 chronology (Brauer et al., 2000b). A reliable error estimate for this interpolated  
201 interval is difficult to determine (Brauer et al., 2014).

### 202 3.2. Tephrostratigraphy and correlation of tephra layers

203 Figure 2 shows the results of cryptotephra investigations in Meerfelder Maar. Throughout  
204 most of the core tephra glass shards were found in discrete layers, or restricted zones, with  
205 low concentrations ( $< 200$  s/g). However, between  $\sim 900 - 700$  cm depth, tephra counts are  
206 much higher. This zone of increased shard counts begins with the visible ( $> 10$  cm thick)  
207 Laacher See Tephra layer (MFM\_876), and continues through the Younger Dryas sediments.  
208 No evidence of background tephra material, from the Meerfelder Maar crater itself, was  
209 observed. Samples of Meerfelder Maar tephra reveal shards densely packed with microlites  
210 and visually very different to those observed reported in this study. In total, 17 layers  
211 containing tephra were studied at 1 cm resolution, and these are labelled in Figure 2  
212 according to their depth. Beginning at the base of the core, the size (longest axis length),  
213 appearance and chemical composition (normalised values) of each of these tephra layers is  
214 described here.

215 Of the 17 tephra samples studied from the Meerfelder Maar sediments, only four can be  
216 confidently correlated to known eruption events and one other correlated to a volcanic  
217 source (Table 3, Figures 4 - 5). Section 3.2 discusses the issues and difficulties involved in  
218 correlating some of the unidentified tephra layers.

219 MFM\_T1137 (1137 cm; before the onset of continuous varve formation):

220 The oldest tephra layer in the Meerfelder Maar core, with a concentration of 50 s/g, shows  
221 both morphological and chemical variability. Most of the glass shards are thin, with  
222 curvilinear form representing bubble-wall junctions. Longest axis lengths are  $< 150 \mu\text{m}$ .  
223 However there are also a number of distinct and smaller glass shards, showing either  
224 deformed and elongated vesicle textures, a high number of un-expanded vesicles and also  
225 some containing microlites ( $< 5 \mu\text{m}$ ).

226 Four glass shards were analysed on the microprobe, all of rhyolitic composition (Table 1 and  
227 Figure 4a). Three of these have 71.2-71.8 wt% SiO<sub>2</sub>, 13.9-14.9 wt% Al<sub>2</sub>O<sub>3</sub>, 1.8-2.3 wt% CaO  
228 2.7-3.9 wt% Na<sub>2</sub>O, 3.5-3.9 wt% K<sub>2</sub>O and are likely to have derived from the same eruption  
229 event. The fourth shard has a much higher SiO<sub>2</sub> content of 77.1 % and lower values of FeO,  
230 MgO and CaO.

231 MFM\_T1130 (1130 cm; before the onset of continuous varve formation):

232 MFM\_T1130 has only 32 s/g, which is the lowest concentration in the core. Glass shards are  
233 dominantly < 120 µm, blocky in appearance and have no internal vesicles, however a small  
234 number of 120-150 µm plate-like glass shards were noted as well as two highly vesicular  
235 shards < 40 µm. Of the nine shards analysed by WDS-EPMA, four show a homogeneous  
236 phonolitic composition, with 57.4-60.8 wt% SiO<sub>2</sub>, 20.0-20.7 wt% Al<sub>2</sub>O<sub>3</sub>, 2.1-2.6 wt% FeO, 5.1-  
237 6.2 wt% Na<sub>2</sub>O and 7.5-8.9 wt% K<sub>2</sub>O. This composition is consistent with that of MFM\_T876.  
238 The remaining shards show a range of rhyolitic compositions (Table 1 and Figure 4a), which  
239 are not interpreted to represent a single volcanic event.

240 MFM\_T1072 (1072 cm; 14,230 ± 90 varve yrs BP):

241 This tephra material is found in the first sample directly after the onset of continuous varve  
242 preservation. Tephra glass shards in MFM\_T1072 are all < 70 µm and have irregular  
243 vesicular forms displaying closed, expanded and elongated vesicles. Glass shard  
244 concentrations were 113 s/g. With the exception of three rhyolitic outliers, the glass shards  
245 from MFM\_T1072 show a bi-modal phono-trachyte to trachyte composition (Table 1, Figure  
246 4). The phono-trachyte end member has 57.3-59.3 wt% SiO<sub>2</sub>, 4.2-5.3 wt% FeO, 0.9-1.5 wt%  
247 CaO, 3.4-3.8 wt% Na<sub>2</sub>O and 7.8-8.9 wt% K<sub>2</sub>O. The trachyte end-member has 61.3-62.0 wt%  
248 SiO<sub>2</sub>, 2.5-3.3 wt% FeO, 2.2-2.5 wt% CaO, 3.5-4.3 wt% Na<sub>2</sub>O and 8.7-9.4 wt% K<sub>2</sub>O. Trace  
249 element analysis of these two end-member compositions show consistent values of ~320  
250 ppm Rb, ~30 ppm Y, ~300 ppm Zr, ~45 ppm Nb and clear bi-modality in Sr (trachy-phonolite  
251 ~900 ppm, trachyte 460 ppm) and Ba (phono-trachyte ~1570 ppm, trachyte 780 ppm). As  
252 shown in Figure 4b, MFM\_T1072 correlates to the Neapolitan Yellow Tuff; generated by a  
253 Plinian eruption from the Campi Flegrei Volcanic Zone (CFVZ) in Southern Italy ~14.2 ka BP  
254 (Section 4.3).

255 The CFVZ was highly active during the Lateglacial and many tephra layers were widely  
256 dispersed that have trachyte to phonolite glass compositions (Siani et al., 2004; Wulf et al.,  
257 2004; Smith et al., 2011). The Neapolitan Yellow Tuff can be distinguished from other CFVZ  
258 eruptions as it straddles the phono-trachyte boundary (Figure 4a) and is composed of two  
259 members: a compositionally bi-modal *lower member* and an *upper member* that spans the  
260 full compositional range between the two lower member populations (Tomlinson et al.,  
261 2012). MFM\_T1067 is chemically correlated to the bi-modal lower member of the  
262 Neapolitan Yellow Tuff, which is consistent with other distal occurrences in Austria and  
263 Slovenia, where only the lower member is found (Schmidt et al., 2002; Lane et al., 2011a).

264 MFM\_T876 (876 cm; 12,880 varve yrs BP):

265 This visible tephra layer has been previously correlated to the LST (Brauer et al., 1999) on  
266 the basis of its stratigraphic position and appearance in thin section. The MFM09 cores  
267 preserve 5 cm of tephra, with a sharp basal contact at 876 cm. Glass shards have very high  
268 vesicularity, characteristic of the LST, which appears like microscopic pumices, with grain  
269 sizes < 300 µm. The 10 cm layer has a homogeneous phonolite composition (Figure 4c), with

270 58.9-63.2 wt% SiO<sub>2</sub>, 18.8-21.2 wt% Al<sub>2</sub>O<sub>3</sub>, 1.1-2.3 wt% CaO and variable alkali contents, 4.9-  
271 9.3 wt% Na<sub>2</sub>O and 6.6-9.0 wt% K<sub>2</sub>O. Trace element analysis of two shards also show  
272 compositions of 183 and 198 ppm Rb, 224 and 334 ppm Sr, 15 and 16 ppm Y, 452 and 466  
273 ppm Zr and 93 and 104 ppm La (Table 2; Figure 4c). Comparison to compositional data  
274 generated on pumice glasses from proximal LST deposits shows that MFM\_T876 correlates  
275 to the Upper phase of the LST, which is the only phase believed to have distributed ash to  
276 the west of the eruption centre in the East Eifel region (van den Bogaard and Schmincke,  
277 1985; Riede et al., 2011).

278 Tephra from the LST continued to be input into the Meerfelder Maar sediments for about  
279 1600 years after the eruption. Concentrations of morphologically and geochemically  
280 identical tephra glass shards are seen to decrease upward within the ~70 cm above the  
281 appearance of the LST at 876 cm, and trace amounts (>100 s/g) are present throughout the  
282 full length of the Younger Dryas sediments.

283 MFM\_T801 (801 cm; 12,140 varve yrs BP):

284 High concentrations of glass shards, ~7060 s/g, were found at 801 – 775.5 cm depth. The  
285 layer is composed of colourless shards with plate-like and curvilinear forms, <200 µm, as  
286 well as light to dark brown shards, <130 µm, with many expanded and some elongate  
287 vesicles.

288 Excluding one shard (EPMA #29, Table 1) that has a phonolitic composition consistent with  
289 MFM\_T876, major and trace element analysis of MFM\_T801 (n=40 and n=15 respectively)  
290 show a bi-modal composition. One end member shows a trend from basaltic-andesite to  
291 andesite (52.8-61.9 wt% SiO<sub>2</sub>, 8.4-13.1 wt% FeO, 4.9-10.5 wt% CaO and 1.1-2.4 wt% K<sub>2</sub>O)  
292 and the second end-member is a homogeneous rhyolite (71.8-72.5 wt% SiO<sub>2</sub>, 3.6-4.0 wt%,  
293 FeO, 1.3-1.5 wt% CaO and 4.5-5.5 wt% K<sub>2</sub>O). Trace element compositions also describe bi-  
294 modality, with approximately 80-90 ppm Rb, 850-950 ppm Zr and 120-130 ppm Nb in the  
295 rhyolitic end member and approximately 30-50 ppm Rb, 350-560 ppm Zr and 50-80 ppm Nb  
296 in the basaltic-andesite member (Figure 4d).

297 Bimodal MFM\_T801 is correlated to the rhyolitic and intermediate phases of the Vedde Ash  
298 (Figure 4d) (Lane et al., 2013), however the Vedde Ash basaltic end-member was not found  
299 in MFM. The Vedde Ash is an important tephra isochron found widely across Europe and the  
300 North Atlantic, erupted from the Katla volcano in Iceland, occurring midway through the  
301 Younger Dryas in many European sediment records (Mangerud et al., 1984; Lane et al.,  
302 2012b), and within Greenland Stadial 1 in the NGRIP ice core (Mortensen et al., 2005;  
303 Rasmussen et al., 2006). MFM\_T801 represents the first appearance within the record of  
304 any shards with Katla Vedde-type composition.

305 MFM\_T711 (711cm; 11,000 varve years BP):

306 A tephra layer found at 710-711 cm depth has previously been correlated to the Ulmener  
307 Maar tephra, dated to 11,000 varve years BP (Zolitschka et al., 1995; Brauer et al., 1999), on  
308 the basis of its appearance and stratigraphic position. This tephra layer contains no typical  
309 aphyric tephra glass shards, but rather crystal-rich juvenile fragments, which are  
310 distinctively isotropic (glassy) but range in shape from rounded to sub-angular, indicating  
311 formation within a very crystal rich melt. Volcanic crystals (pyroxene, olivine, mica, oxide  
312 minerals) and lithic fragments are also present within the denser fraction of the separated  
313 sample. Grain sizes of all fractions are < 90 µm. This texture is consistent with other samples

314 of the UMT taken from proximal outcrops, where pumice clasts are holocrystalline. In the  
315 absence of areas of aphyric glass, no chemical analysis was made on this tephra layer.

316 MFM\_T687 (687 cm; 10,648 varve yrs BP) & MFM\_T685 (685 cm; 10,619 varve yrs BP):

317 Tephra concentrations decrease dramatically at ~730 cm during the first centuries of the  
318 Holocene (Figure 2) and associated with climatic amelioration and resultant increase in  
319 vegetation cover and stabilisation of the landscape in and around the Meerfelder Maar  
320 catchment. The first appearance of tephra glass shards in the Holocene is of concentrations  
321 of 3 – 232 s/g found between 678 and 667 cm. From this zone of tephra, two 1 cm samples  
322 with the highest shard concentrations were picked out for analysis. Both MFM\_T687 (232  
323 s/g) and MFM\_T685 (113 s/g) are dominated by highly vesicular tephra shards, <70 µm,  
324 which have both morphological and chemical affinity to MFM\_T876 (Figure 4). In both  
325 samples, a smaller number of <120 µm plate-like shards are also present, and these are  
326 represented by a number of rhyolitic major and trace element analyses from MFM\_T685.

327 Thin section analysis of the sediments around 685-687 cm revealed a number of fine  
328 minerogenic detrital layers, which are interpreted as extreme runoff events (Martin-Puertas  
329 et al., 2012b; van Geel et al., 2013). It suggests these layers are not formed from volcanic  
330 airfall events, but from reworking of older tephra-bearing sediment within the Meerfelder  
331 Maar catchment.

332 MFM\_T573 (573 cm; 7,744 varve yrs BP):

333 Glass shard concentrations in MFM\_T573 are 92 s/g. Tephra glass shards are < 80 µm and  
334 fairly blocky in shape, with concave edges from fragmented vesicle walls. Four analyses  
335 were achieved on these small shards and reveal peralkaline pantellerite compositions  
336 (following Macdonald, 1974), with 69-75 wt% SiO<sub>2</sub>, 6.1-7.5 wt % Al<sub>2</sub>O<sub>3</sub>, 3.0-4.7 wt % FeO,  
337 1.6-1.8 wt % MgO, 1.8-3.0 wt% CaO, 5.6-6.1 wt% Na<sub>2</sub>O and 6.5-8.7 wt% K<sub>2</sub>O. Just one LA-  
338 ICP-MS analysis was made on a pantellerite glass shard and this has approximately 220 ppm  
339 Rb, 30 ppm Zr, 11 ppm Nb and 349 ppm Ba (Table 2). Also within this sample there are a  
340 number of highly vesicular shards, <200 µm, of phonolitic composition consistent with  
341 MFM\_T876 (MFM\_T573, #1-8 in Table 1) and two more platy shards (MFM\_T573, #9-10  
342 Table 1) with rhyolitic major, minor and trace element compositions consistent with  
343 MFM\_T801.

344 Pantellerite tephra are rare and commonly come from volcanic centres associated with  
345 continental or ocean ridge rifting (Civetta et al., 1984). In Europe and the North Atlantic,  
346 Holocene Pantellerites have been reported from Pantelleria Island in the Mediterranean  
347 (Mahood and Hildreth, 1986; Magny et al., 2011) and Jan Mayen in the North Atlantic  
348 (Lacasse and Garbe-Schönberg, 2001). Terceira volcano in the Azores has also erupted  
349 peralkaline trachytes (Gertisser et al., 2010). However, the available glass data from these  
350 volcanic centres does not correlate with MFM\_T573 (Figure 4e), therefore the source  
351 eruption remains unidentified.

352 MFM\_T568 (568 cm; 7,633 varve yrs BP):

353 Distinctly plate-like shards, < 50 µm in size, characterise MFM\_T568. A concentration of 75  
354 s/g was calculated from a small sample size of only 0.04g, therefore although replicable;  
355 only 3 shards were counted in the original 1 cm sample. A single shard was analysed by  
356 WDS-EPMA and had a rhyolitic composition consistent with MFM\_T801.



357 MFM\_T552 (552cm; 7,314 varve yrs BP), MFM\_T550 (550 cm; 7,279 varve yrs BP)&  
358 MFM\_T548 (548 cm; 7,245 varve yrs BP):

359 Low concentrations (<20 s/g) of tephra were observed in the low resolution (10 cm) scans  
360 between 484 and 540 cm depth (Figure 2). At 1 cm resolution, tephra was seen to be  
361 present through much of this depth, again in concentrations <20 s/g. The three samples  
362 with the highest shard concentrations were found at 527-548 cm (50 s/g), 529-550 cm (38  
363 s/g) and 531-552 cm (61 s/g). These three samples were selected for analysis. All three  
364 layers contained equant and platy tephra shards with curvilinear surfaces, < 90 µm.  
365 MFM\_T552 and MFM\_T548 also contained < 40 µm shards with many expanded vesicles.  
366 EMPA was only possible on five shards from across these three samples and did not reveal  
367 any consistent chemical compositions. The glass shard in MFM\_T552 is an alkali-trachyte,  
368 which plots close to the composition of MFM\_T1067 on elemental bi-plots (Figure 4a). Two  
369 shards, one in each of MFM\_T550 and MFM\_T548, correlate to MFM\_T876. A rhyolitic  
370 shard was also found in MFM\_T550 and another alkali-trachytic shard was measured in  
371 MFM\_T548.

372 MFM\_T334 (334 cm; 3,382 varve yrs BP):

373 Tephra glass shards in MFM\_T334 are <50 µm in their longest axis and very thin, with  
374 curved shapes and closed circular and irregular vesicles. Very fine microlites (< 10 µm) were  
375 noted in a couple of shards. Glass shard concentrations were 113 s/g. Three trachytic glass  
376 shards were analysed from this sample, with approximately 62.5-64.6 % SiO<sub>2</sub>, 16.6-18.0 wt  
377 % Al<sub>2</sub>O<sub>3</sub>, 3.9-4.4 wt% FeO, 7.3-8.3 wt% Na<sub>2</sub>O and 4.9-5 wt % K<sub>2</sub>O. One shard is distinct as it  
378 has a higher CaO content of 1.7 wt% and this differentiation is also evident in the trace  
379 element composition (Tables 1 and 2). As apparent in Figure 4e the compositions of the  
380 remaining two shards from MFM\_T334 show some similarity to Late Holocene tephra layers  
381 found in Western Ireland, in the sites of Loch Mor, Inis Oirr (Chambers et al., 2004) and  
382 Derrycunihy (Reilly and Mitchell, 2014). The tephra layers in Loch Mor have been correlated  
383 to trachytic eruptions from Jan Mayen, however they are much younger than MFM\_T334,  
384 being dated to between AD 1400 and AD 1915. At Derrycunihy, tephra with a similar  
385 composition has been tentatively correlated to the Mt Furnas volcano in the Azores and this  
386 may in fact offer a better correlation for many of the cryptotephra currently correlated to  
387 Jan Mayen in Western Ireland (Reilly and Mitchell, 2014; Johannesson, in press). The  
388 available summary glass data from Mt Furnas is plotted in Fig. 4 and it is anticipated that  
389 forthcoming data will secure the correlation of MFM\_T334 to an eruption of this Azores  
390 volcano.

391 MFM\_T325 (325cm; 3,230 varve yrs BP):

392 Thin, curvilinear glass shards with open vesicles, < 90 µm long, were found in a  
393 concentration of 100 s/g at 325 – 320 cm. However, no shards were successfully recovered  
394 for chemical analysis from this layer (Section 3.2).

395 MFM\_T322 (322 cm; 3,162 varve yrs BP):

396 This tephra layer contained highly vesicular shards, <60 µm, similar in morphology to the  
397 LST. A glass shard concentration of 63 s/g was found. Again, extraction of tephra shards  
398 from this layer for geochemical analysis was unsuccessful.

399 MFM\_T238 (238 cm; 2,020 varve yrs BP):

400 Tephra glass shard concentrations of 90 s/g and 72 s/g were found in 1 cm samples from  
401 238 – 239 cm and 237 – 238 cm, respectively. Across these two samples the shard  
402 morphologies were very similar, with large (< 150 µm) irregular forms, containing either  
403 small closed circular vesicles or expanded vesicle forms. Due to the high organic content of  
404 these samples, the absolute number of shards observed in each 1cm sample was 13 and 9,  
405 respectively; these samples were therefore combined for geochemical analysis. The two  
406 resultant WDS-EPMA analyses reveal two different trachytic compositions, as evident in  
407 Table 1 and Figure 4a.

### 408 3.2. Unidentified tephra samples

409 12 of the cryptotephra layers located within MFM remain unattributed to a volcanic source  
410 or a specific eruption event. The reasons for this include insufficient chemical analysis due  
411 to the small shard concentrations (e.g. MFM\_T568), heterogeneous compositions (e.g.  
412 MFM\_T1130) and a lack of correlative data (e.g. MFM\_T334). Tephra shards with  
413 compositions that correlate to the Vedde Ash or Laacher See Tephra (MFM\_T889 or  
414 MFM\_T801) are found intermittently throughout the record and these may indicate re-  
415 deposition of tephra from within the maar catchment. In the case of MFM\_T687 and  
416 MFM\_T685, detrital layers have been identified by thin section analysis.

417 Nevertheless, multiple eruptions from Katla have been shown to deliver compositionally  
418 similar tephra layers to northern Europe (Wastegård, 2002; Koren et al., 2008; Matthews et  
419 al., 2011; Lane et al., 2012b) and this could also explain the presence of tephra shards with a  
420 Vedde Ash-like rhyolite composition. MFM\_T568 for example, which is dated to ca 7617  
421 varve yrs BP may be correlated to the Suduroy tephra, described by Wastegård (2002) from  
422 the Faroe Isles and dated to 8308 - 7868 cal years BP ( $7240 \pm 95$  14C years, calibrated in  
423 OxCal v4.1 using the IntCal13 calibration curve (Bronk Ramsey, 2001; Reimer et al., 2013).  
424 Correlations based upon a few isolated shards are however, not robust. This is exemplified  
425 by the scatter within some samples (e.g. MFM\_T573), which illustrates the need for multiple  
426 analyses to build a complete picture of a tephra sample's chemical composition. Such mixed  
427 populations could of course come from more than one eruption event, closely spaced in  
428 time. Samples were taken at 1 cm resolution, which represents approximately 20 - 30 years  
429 of sedimentation.

430 Finally, it is of course possible that some tephra layers were missed altogether, either due to  
431 the presence of cm-scale gaps between individual core segments of MFM09, or due to  
432 patchy preservation within the lake floor sediments.

433

## 434 4. Discussion

### 435 4.1. A new tephrostratotype sequence for Europe

436 The preservation of multiple tephra layers within an annually resolved archive establishes  
437 the Meerfelder Maar Lateglacial sediment record as a key tephrostratotype site (Figure 5).  
438 By providing high precision varve ages for co-located tephra layers from different volcanic  
439 centres, Meerfelder Maar provides an important chronological contribution to the existing  
440 tephrostratigraphic framework that connects sites from the North Atlantic to the  
441 Mediterranean (Davies et al., 2012; Lane et al., 2012a)

442 The four tephra layers successfully identified in Meerfelder Maar record eruptions from  
443 three different volcanic centres: the nearby Eifel volcanic zone (West and East Eifel); Katla,  
444 in the eastern volcanic zone of Iceland; Campi Flegrei volcanic zone, in Southern Italy. With  
445 the exception of the Ulmener maar tephra, which is less widespread, the tephra layers  
446 facilitate direct correlations between a large number of palaeoenvironmental archives from  
447 across Europe and the North Atlantic (Figure 6).

448 Of particular note is the discovery of the Neapolitan Yellow Tuff in Western Germany, ~1200  
449 km from the source in Campi Flegrei. The Neapolitan Yellow Tuff isochron allows the  
450 Meerfelder Maar record to be directly linked to the varve record of Lago Grande di  
451 Monticchio in Southern Italy (Wulf et al., 2004) (Figure 6), a discontinuously varved  
452 sediment record of Mediterranean environmental change spanning approximately 133 ka  
453 (Brauer et al., 2007). This discovery therefore highlights the potential for making high-  
454 precision comparisons of the phasing of environmental transitions between Lateglacial  
455 sediment records from Central Europe and the Mediterranean.

#### 456 4.2. Addressing the unknowns

457 A number of important points with regards to the limitations of characterising cryptotephra  
458 layers are highlighted by the number of unattributed cryptotephra layers in Meerfelder  
459 Maar (13 of 17).

460 Primarily, it is evident that our existing knowledge of widespread tephra layers is  
461 incomplete, even for a region and time period as well-studied as the European Lateglacial  
462 and Holocene. In the case of some layers, e.g. MFM\_T334, volcanic sources can be  
463 tentatively attributed, but for others no correlation is suggested. The addition of 51 well-  
464 defined tephra isochrons (16 Icelandic, 17 Italian, 9 Massif Central, 3 Eifel, 2 Hellenic Arc, 3  
465 Anatolian and 1 Carpathian) to the latest INTIMATE event stratigraphy back to 60,000 years  
466 BP (Blockley et al., 2014) illustrates the focus of European cryptotephra research on archives  
467 dominated by Icelandic and Italian tephra layers. This in part reflects the prevalence of far  
468 travelled tephra from these volcanic regions during the Lateglacial, but also highlights that  
469 detailed studies, generating compatible tephra glass shard compositional data, are much  
470 needed from other volcanic regions of Europe (e.g. the Massif Central, Azores).

471 Secondly, the majority of unattributed tephra layers contain low concentrations of glass  
472 shards of variable rhyolitic compositions (e.g. MFM\_T1137, MFM\_T 1130, MFM\_T573,  
473 MFM\_T568, MFM\_T550; outliers in MFM\_T1072). Rhyolitic magmas are common in the  
474 European record, being frequently generated from volcanoes in Iceland, the Aegean, the  
475 Aeolian Islands, the Carpathians and Central Anatolia (Tomlinson et al., in press). Typically  
476 rhyolites are erupted during highly explosive eruptions (sub-plinian to plinian) and are  
477 characterised by bubble-wall to plate-like glass shards. This material is therefore able to be  
478 transported extreme distances in the atmosphere and the sources for these tephra shards  
479 may be far beyond the volcanic centres of Europe. Whilst comparisons to all available  
480 datasets have been made in attempt to identify the unattributed tephra shards from  
481 Meerfelder Maar, the small concentrations and often variable compositions suggest that  
482 robust correlations are not likely for many of the layers. Trace element analyses could be  
483 used to help narrow down the source region of these glasses (e.g. Tomlinson et al., in press),  
484 however larger datasets would be needed than are available here.

485 Finally, the importance of both robust compositional characterisation and a good  
486 understanding of taphonomy of cryptotephra layers are highlighted by this study. Working

487 in the undisturbed laminated sections of the Meerfelder Maar sequence, for which detailed  
488 thin section micromorphology has been carried out, has allowed the recognition of at least  
489 one area of the core where tephra has been reworked and later re-deposited within the lake  
490 sediments. Thin section analyses confirmed that tephra shards, found in concentrations of  
491 <232 s/g between 690-684 cm, are located coincident with fine detrital material, indicating  
492 these are reworked deposits (section 3.1). This was supported by EMPA of MFM\_T687 and  
493 MFM\_T685, which turned out to be composed of tephra glass shards from the LST and VA  
494 eruptions. Critically, this reworking event was only confirmed by the thin section work,  
495 whereas within a less well-studied sediment sequence, the layers may have been  
496 considered as genuine air fall tephra layers. Indeed, it may be the case that some of the  
497 remaining Holocene tephra layers in the Meerfelder cores could also represent reworked  
498 wind-blown or in-washed tephra.

#### 499 4.3. Improved dating of eruptions and events

500 Table 3 provides varve age estimates for the Ulmener Maar tephra (UMT), Vedde Ash (VA),  
501 Laacher See tephra (LST) and Neapolitan Yellow Tuff (NYT), all of which were found within  
502 the varved portion of the Meerfelder Maar record. These ages agree with independently  
503 generated age estimates for each of the eruptions and in the case of the NYT significantly  
504 improve on the existing dating precision. The Neapolitan Yellow Tuff has been dated by the  
505  $^{40}\text{Ar}/^{39}\text{Ar}$  method to  $14.9 \pm 0.4$  ka (Deino et al., 2004). This age, however, is older than ages  
506 obtained by radiocarbon dating of proximal and distal material associated with this ash  
507 (Blockley et al., (2008) and predates an IntCal-13 (Reimer et al., 2013) modelled date of  
508 14,366 - 14,022 cal BP by (Bronk Ramsey et al., in press-a), obtained by Bayesian  
509 combination of radiocarbon age-estimates from multiple sites. The Neapolitan Yellow Tuff is  
510 also located in Lago Grande di Monticchio, southern Italy, where it is varve dated to  $14,120$   
511  $\pm 710$  yrs BP (Wulf et al., 2008). The revised Meerfelder Maar chronology (MFM-2014)  
512 presented in this paper dates the NYT at  $14,230 \pm 90$  varve yrs BP. The NYT in MFM is  
513 located at the boundary between discontinuous and poor varve preservation of the early  
514 Lateglacial interstadial and continuous preservation of distinct varves that is related to the  
515 stabilisation of the catchment by vegetation cover. Differential dating between the most  
516 important Lateglacial and early Holocene tephra layers in MFM reveals  $1350 \pm 50$  varve yrs  
517 between the NYT and the LST,  $740 \pm 40$  varve yrs between the LST and the VA, and  $1140 \pm$   
518  $40$  varve yrs between the VA and the UMT. This information can be imported into other  
519 archives containing two or more of these tephra layers and used to increase age model  
520 precision and accuracy.

521 Varve counting between each of the tephra layers and regional biostratigraphical  
522 boundaries preceding and post-dating them, helps to explore the timing and duration of  
523 some the local palaeoenvironmental responses to widely observed climatic transitions  
524 (Table 3). These differential ages can be compared to other high resolution archives  
525 containing the same tephra layers and precise assessments of the synchronicity of local  
526 environmental transitions can be made. Whilst some tephra layers have a limited dispersal,  
527 such as the UMT, which occurs 590 years after the transition into the Holocene, others such  
528 as the VA, can be correlated over continental distances.

529 The relative durations of GS-1 (Greenland) and the Younger Dryas (Europe) have been  
530 discussed previously (Brauer et al., 1999; Brauer et al., 2008; Muscheler et al., 2008; Lane et  
531 al., 2011b; Lohne et al., 2013), however, even annually resolved records suffer from decadal  
532 to centennial-scale uncertainties that have prevented precise comparisons of abrupt

533 transitions. The Vedde Ash provides a means of directly synchronising the Meerfelder varve  
534 chronology with GICC05, facilitating precise comparison of the timing of the Younger Dryas  
535 in Meerfelder Maar and GS-1 in NGRIP for the first time (Table 3). The Younger Dryas in  
536 Meerfelder Maar (12,679-11,590 varve years BP) began 539 varve years before the  
537 deposition of the Vedde Ash and the transition into the Holocene occurred 550 years  
538 afterwards (Table 3). These transitions are defined by major biostratigraphical boundaries  
539 (Litt and Stebich, 1999) accompanied by abrupt changes in sediment proxies of Meerfelder  
540 Maar (Brauer et al., 1999). Using the GICC05 chronology, the GS-1 onset and end in NGRIP  
541 are defined by the deuterium excess record ( $\delta D - 8\delta^{18}O$ ), which records abrupt shifts within  
542 1-3 years (Rasmussen et al., 2006; Steffensen et al., 2008). The Vedde Ash (12,171  $\pm$ 114 b2k)  
543 in NGRIP lies 725 GICC05 years after the start and 468 GICC05 years prior to the end of GS-1  
544 (Table 3). Accepting both of the chronologies as correct implies that the onset of GS-1 in  
545 NGRIP leads the onset of the Younger Dryas in Meerfelder by 186 years and also leads at the  
546 start of the Holocene by 132 years. Refining the correlation between these important  
547 Lateglacial archives provides a sound platform from which the nature of abrupt climate  
548 changes over continental distances and the complexities of environmental proxy  
549 sensitivities can be explored (e.g., Lane et al., 2013; Rach et al., 2014)

## 550 5. Conclusions

551 Meerfelder Maar now stands out as an important Western European tephrostratotype  
552 record for the Lateglacial, providing improved age estimates for, and precise dating of  
553 intervals between, tephra layers from three different volcanic centres. Using tephra layers  
554 as tie-points between Meerfelder Maar and other archives with annual to decadal-scale  
555 chronological resolution has allowed, for the first time, precise layer-counted comparisons  
556 between the timing and duration of regional palaeoclimate signals across Europe and the  
557 North Atlantic. These results contribute to a better understanding of proxy-response to  
558 complex climate forcing events (Lane et al., 2013; Rach et al., 2014). There remains great  
559 potential for extending these correlations to other sites containing the Vedde Ash, Laacher  
560 See Tephra and Neapolitan Yellow Tuff, as suitably high-resolution palaeoenvironmental  
561 records are produced. Furthermore, as detailed records emerge from less well-studied  
562 volcanic centres, it is envisaged that some of the unattributed cryptotephra within the  
563 Meerfelder Maar record will be identified and will provide additional valuable marker layers  
564 for the correlation of Lateglacial and Holocene records.

## 565 6. Acknowledgements

566 This study is a contribution to the INTIMATE project (INTEgrating Ice core, MARine and  
567 TERrestrial records, <http://intimate.nbi.ku.dk/>); and the climate initiative REKLIM Topic 8  
568 "Abrupt climate change derived from proxy data" of the Helmholtz Association (A.B. and  
569 C.M.-P.). The research was funded by the UK Natural Environment Research Council  
570 consortium RESET (NE/E015670/1 and NE/E015905/1). C.S.L. was partly funded by the  
571 Leverhulme Trust. This study has used infrastructure of the Terrestrial Environmental  
572 Observatory (TERENO) of the Helmholtz Association. We thank the Maar Museum in  
573 Manderscheid for local support.

574

## 575 7. Tables and Figures

## 576 Table 1:

577 Single-shard major and minor element oxide compositions (wt%) for all tephra layers  
 578 analysed within the Meerfelder Maar record, measured by electron microprobe (section  
 579 2.3). For samples with n>12 analyses, a reduced representative dataset is shown and the full  
 580 dataset is contained within Supplementary Information (Table S1). Data are presented  
 581 normalised to water-free compositions, with original totals shown, after filtering points with  
 582 analytical totals below 94 weight %. Secondary standard data, which provide a measure of  
 583 precision and accuracy, are presented within Supplementary Information (Table S2).

EPMA #	SiO <sub>2</sub>	TiO <sub>2</sub>	Al <sub>2</sub> O <sub>3</sub>	FeO	MnO	MgO	CaO	Na <sub>2</sub> O	K <sub>2</sub> O	P <sub>2</sub> O <sub>5</sub>	Total	Std file
MFM_T1137: before the onset of continuous varve formation												
1	71.82	0.02	13.93	3.53	0.19	1.61	2.28	2.70	3.91	0.00	96.79	a
2	71.20	0.23	14.94	3.22	0.09	1.01	1.75	3.90	3.67	0.01	99.08	a
3	71.27	0.37	14.91	3.12	0.07	1.04	1.77	3.91	3.51	0.02	99.24	e
4	77.09	0.06	12.71	1.05	0.01	0.03	0.56	3.79	4.70	0.00	94.42	e
MFM_T1130: before the onset of continuous varve formation												
1	57.81	0.33	20.14	2.36	0.17	0.67	3.49	6.18	8.81	0.05	96.77	f
2	57.46	0.43	20.00	2.62	0.14	0.94	3.38	6.11	8.92	0.00	97.49	a
3	60.28	0.61	20.46	2.35	0.24	0.32	1.94	5.09	8.58	0.13	96.22	a
4	60.79	0.57	20.66	2.06	0.14	0.27	2.17	5.77	7.46	0.10	99.53	a
5	71.83	0.62	11.53	4.04	0.05	1.21	0.25	2.82	7.61	0.04	95.60	f
6	71.17	0.45	13.14	4.19	0.14	1.52	2.61	2.67	4.04	0.08	98.05	g
7	74.60	0.12	12.17	2.15	0.01	0.81	0.89	2.55	6.70	0.01	95.50	g
8	76.89	0.04	12.88	0.90	0.13	0.04	0.59	3.84	4.64	0.03	95.19	f
MFM_T1072: 14,230 varve yrs BP												
1	57.34	0.61	18.67	5.33	0.10	1.50	4.51	3.80	7.83	0.30	94.91	f
3	57.71	0.59	19.18	4.72	0.04	1.30	4.24	3.53	8.36	0.32	97.62	e
5	58.10	0.58	18.80	4.84	0.11	1.37	4.16	3.44	8.30	0.31	96.23	a
7	58.30	0.59	18.66	4.78	0.13	1.17	3.95	3.82	8.33	0.28	94.12	f
9	58.93	0.48	18.92	4.28	0.14	1.13	3.78	3.59	8.46	0.29	97.74	a
11	61.35	0.42	18.51	3.31	0.10	0.62	2.52	3.91	9.16	0.11	94.51	e
13	61.80	0.49	18.76	2.92	0.18	0.44	2.26	4.29	8.77	0.10	97.28	a
15	62.02	0.43	18.80	2.98	0.22	0.40	2.24	4.10	8.72	0.09	96.88	f
16	62.19	0.39	18.91	2.53	0.12	0.41	2.21	4.09	9.08	0.08	95.62	a
17	75.14	0.15	14.16	1.74	0.05	0.76	1.15	2.44	4.13	0.29	96.60	f
18	72.34	0.59	12.92	3.64	0.24	1.98	1.68	3.20	3.38	0.02	99.46	f
19	77.08	0.14	11.82	2.38	0.08	0.02	0.69	4.41	3.38	0.01	96.26	f
MFM_T876: 12,880 varve yrs BP												
1	58.91	0.29	21.21	2.22	0.11	0.18	1.09	9.33	6.64	0.03	97.19	e
3	59.49	0.37	20.74	2.26	0.10	0.20	1.40	8.44	6.96	0.04	97.36	e
5	59.72	0.57	20.34	2.56	0.08	0.24	1.96	6.70	7.78	0.06	98.51	e
7	59.88	0.58	20.08	2.45	0.09	0.30	1.93	6.68	7.90	0.10	96.06	e
9	60.41	0.57	20.05	2.36	0.11	0.28	1.75	6.73	7.70	0.05	98.36	b
11	60.53	0.57	20.02	2.08	0.09	0.25	1.71	6.86	7.82	0.08	97.31	e
13	60.56	0.40	20.18	2.36	0.07	0.25	1.74	6.95	7.43	0.05	98.20	e
15	60.60	0.57	20.16	2.24	0.06	0.16	1.37	7.57	7.20	0.08	96.85	e
17	60.86	0.55	19.78	2.49	0.22	0.27	2.03	5.75	7.98	0.08	96.22	b
19	63.19	0.33	19.62	1.26	0.07	0.12	1.49	4.87	9.03	0.03	99.07	b
MFM_T801: 12,140 varve yrs BP												
1	52.88	3.58	13.61	12.26	0.21	3.93	8.18	3.45	1.36	0.54	96.93	c
5	53.21	3.44	13.47	12.70	0.28	3.81	8.17	3.15	1.32	0.46	97.52	c
9	55.01	3.23	13.52	11.54	0.19	3.50	7.20	3.81	1.57	0.43	98.42	c
13	55.39	3.17	13.64	11.28	0.15	3.49	7.27	3.61	1.56	0.44	97.23	c
21	56.93	2.88	13.36	10.92	0.12	3.29	6.95	3.60	1.61	0.34	97.68	d
25	58.43	2.25	14.30	9.48	0.19	2.60	5.98	4.38	1.73	0.67	98.30	c
29	60.39	0.60	20.17	2.26	0.09	0.29	1.82	6.50	7.83	0.06	97.02	c
34	71.78	0.34	13.39	3.95	0.14	0.22	1.36	5.34	3.40	0.08	97.05	d
38	72.15	0.27	13.60	3.68	0.18	0.20	1.43	5.00	3.49	0.01	98.22	d
40	72.50	0.28	13.79	3.80	0.18	0.21	1.28	4.49	3.46	0.03	96.67	d

		SiO <sub>2</sub>	TiO <sub>2</sub>	Al <sub>2</sub> O <sub>3</sub>	FeO	MnO	MgO	CaO	Na <sub>2</sub> O	K <sub>2</sub> O	P <sub>2</sub> O <sub>5</sub>	Total	Std file
MFM_T687:10,648 varve yrs BP													
	1	58.90	0.92	20.10	2.87	0.03	0.33	2.42	6.54	7.78	0.12	96.57	e
	5	60.13	0.60	20.16	2.35	0.04	0.32	1.87	6.59	7.88	0.07	96.41	e
	9	59.43	0.37	21.23	1.92	0.21	0.15	1.60	8.46	6.56	0.06	97.78	a
	13	60.28	0.57	20.05	2.50	0.21	0.32	1.75	7.02	7.23	0.07	96.86	a
	17	59.27	0.74	20.01	2.90	0.17	0.44	2.26	6.88	7.23	0.10	98.78	a
	30	60.13	0.50	20.26	2.23	0.10	0.31	1.83	6.64	7.94	0.08	98.14	e
	34	60.21	0.48	20.37	2.27	0.15	0.29	1.82	6.74	7.59	0.08	98.21	a
	38	60.18	0.61	20.03	2.30	0.15	0.33	1.88	6.59	7.86	0.08	98.87	a
	42	60.69	0.42	20.59	2.12	0.14	0.20	1.20	7.35	7.25	0.04	99.02	a
	46	63.95	0.62	18.02	2.42	0.08	0.31	1.49	5.64	7.37	0.11	98.64	a
	47	71.57	0.30	13.95	3.64	0.19	0.24	1.45	5.10	3.47	0.09	97.26	a
	51	71.45	0.27	13.78	3.95	0.14	0.22	1.34	5.27	3.52	0.06	98.85	a
MFM_T685: 10,619 varve yrs BP													
	3	60.07	0.52	20.09	2.52	0.21	0.28	1.65	6.77	7.79	0.08	95.89	c
	5	60.48	0.29	20.71	1.96	0.20	0.18	1.42	7.80	6.89	0.07	96.20	a
	7	59.37	0.63	20.37	2.70	0.14	0.35	2.19	6.29	7.82	0.13	98.25	a
	9	60.20	0.55	20.30	2.26	0.15	0.29	1.82	6.73	7.65	0.07	97.55	c
	11	60.41	0.56	20.25	2.17	0.10	0.27	1.87	6.49	7.68	0.18	97.47	a
	13	60.21	0.60	20.28	2.43	0.18	0.28	1.69	6.82	7.45	0.06	98.19	c
	15	59.88	0.74	20.16	2.76	0.19	0.44	1.82	6.41	7.49	0.12	99.16	a
	17	61.13	0.71	19.60	2.80	0.30	0.35	1.87	6.21	6.96	0.08	97.45	a
	20	60.59	0.45	20.12	2.18	0.12	0.30	1.85	6.64	7.69	0.06	98.97	a
	21	71.63	0.29	13.62	3.70	0.09	0.26	1.37	5.39	3.61	0.03	98.54	e
	22	71.45	0.27	13.78	3.95	0.14	0.22	1.34	5.27	3.52	0.06	98.85	a
	23	75.70	0.27	13.10	1.66	0.06	0.16	0.23	2.53	6.15	0.13	95.85	a
MFM_T573: 7,744 varve yrs BP													
	1	60.40	0.56	19.81	2.41	0.17	0.31	1.95	6.58	7.72	0.09	97.57	g
	2	60.60	0.55	20.02	2.25	0.20	0.31	1.83	6.60	7.55	0.09	97.45	g
	5	60.18	0.47	20.45	2.11	0.17	0.24	1.86	6.73	7.69	0.10	99.33	a
	6	61.29	0.38	20.22	1.77	0.05	0.20	1.72	6.63	7.70	0.04	97.66	g
	7	61.11	0.39	20.52	2.02	0.20	0.21	1.67	6.21	7.60	0.07	98.90	f
	8	62.19	0.33	19.12	2.06	0.13	0.42	1.33	6.26	8.12	0.02	99.28	g
	9	71.81	0.30	13.56	3.76	0.20	0.23	1.36	5.09	3.64	0.06	96.52	g
	10	71.48	0.28	13.50	4.01	0.13	0.21	1.34	5.50	3.50	0.03	97.87	g
	11	69.00	0.69	7.45	4.68	0.11	1.60	1.89	5.93	8.59	0.06	98.65	f
	12	72.21	0.46	7.29	3.38	0.09	1.78	2.71	5.39	6.62	0.08	98.48	g
	13	71.93	0.60	6.69	4.38	0.10	1.72	3.00	5.04	6.51	0.05	98.93	f
	15	75.25	0.11	6.86	3.00	0.05	1.17	2.17	4.56	6.81	0.02	98.94	g
MFM_T568: 7,633 varve yrs BP													
	1	71.76	0.30	13.96	3.69	0.13	0.21	1.37	4.89	3.63	0.06	98.49	a
MFM_T552: 7,314 varve yrs BP													
	1	62.49	0.64	19.03	2.22	0.24	0.34	1.49	6.40	7.04	0.12	100.33	a
MFM_T550: 7,279 varve yrs BP													
	1	60.68	0.61	19.83	2.30	0.19	0.28	1.34	7.95	6.75	0.08	97.18	f
	2	75.26	0.49	13.70	1.33	0.11	0.36	0.46	3.59	4.70	0.02	95.67	f
MFM_T548: 7,245 varve yrs BP													
	1	60.25	0.52	20.10	2.30	0.23	0.25	1.71	7.01	7.58	0.05	98.78	f
	2	63.61	0.27	17.96	3.66	0.27	0.19	0.70	7.98	5.31	0.04	98.33	f
MFM_T334: 3,382 varve yrs BP													
	1	62.49	0.64	17.99	3.92	0.21	0.58	1.67	7.30	5.00	0.20	96.73	f
	2	63.88	0.41	17.16	4.28	0.24	0.28	0.86	7.95	4.87	0.08	97.18	f
	3	64.59	0.21	16.62	4.38	0.22	0.12	0.60	8.33	4.90	0.03	98.00	f
MFM_T238: 3,230 varve yrs BP													
	1	63.87	0.08	19.03	0.96	0.09	0.41	1.78	6.39	7.38	0.01	100.36	a
	2	67.85	0.59	14.73	4.68	0.17	1.88	0.25	2.80	6.86	0.18	99.85	a

585

586

587 Table 2:  
 588 Single-shard trace element compositions (ppm) of tephra layers within the Meerfelder Maar  
 589 record, measured by laser ablation inductively coupled plasma mass spectrometry (section  
 590 2.3). Secondary standard data, which provide a measure of precision and accuracy, are  
 591 presented within Supplementary Information. “<LOD” indicates the element concentration  
 592 was below the limits of detection for that analyses.

	EPMA #	Rb	Sr	Y	Zr	Nb	Ba	La	Ce	Pr	Nd	Sm	Eu	Gd	Dy	Er	Yb	Lu	Ta	Th	U	Std filed	
MFM_T1072: 14,230 varve yrs BP																							
	7	335	863	30	303	47	1482	74	137	16	57	11.6	2.2	<LOD	5.7	2.3	<LOD	<LOD	2.5	25.3	8.6	a	
	4	318	903	29	295	44	1597	71	136	13	59	10.4	2.3	6.3	5.6	2.9	<LOD	0.4	2.1	26.2	7.5	b	
	8	308	926	30	292	44	1643	72	148	13	62	10.8	2.2	4.8	4.6	2.9	2.7	<LOD	2.0	26.2	7.9	b	
	11	321	466	31	324	48	782	65	125	12	52	9.8	2.0	5.7	4.9	2.9	3.4	<LOD	2.3	26.9	8.0	b	
	17	303	227	217	60	6	541	54	110	12	48	11.9	2.2	23.2	39.0	14.7	5.2	0.4	0.5	15.5	11.5	a	
	18	63	158	40	21	13	113	48	98	11	46	10.8	1.4	7.9	7.6	4.0	3.8	0.6	0.6	9.4	2.9	a	
MFM_T876: 12,880 varve yrs BP																							
	4	198	224	16	452	146	265	104	158	13	37	<LOD	<LOD	<LOD	2.3	1.7	2.2	<LOD	6.3	15.7	4.1	b	
	7	183	330	15	466	132	392	93	144	12	35	4.0	1.0	2.4	2.4	1.6	2.2	0.3	5.2	15.0	3.9	b	
MFM_T801: 12,140 varve yrs BP																							
	1	28	396	42	355	50	278	36	83	11	46	10.6	3.2	10.8	8.9	4.3	3.7	<LOD	3.0	3.8	1.2	c	
	2	29	397	46	370	53	296	39	89	11	49	11.1	3.3	10.3	9.5	4.7	3.8	<LOD	3.4	4.2	<LOD	c	
	4	32	395	46	400	56	333	43	95	11	52	10.9	3.3	10.6	10.0	5.4	4.3	<LOD	3.4	4.4	<LOD	c	
	5	32	363	46	393	54	301	40	92	11	47	10.6	2.9	11.2	9.1	4.5	3.7	<LOD	3.3	4.2	<LOD	c	
	7	31	391	44	364	52	289	38	88	11	48	11.8	3.1	11.3	8.9	4.4	4.1	<LOD	3.1	4.1	<LOD	c	
	9	35	388	48	424	58	320	43	96	12	53	12.1	3.2	11.0	9.3	5.0	4.1	<LOD	3.6	4.7	1.5	c	
	10	38	386	51	448	63	358	45	105	12	52	13.2	3.3	10.7	10.3	5.5	4.5	<LOD	3.8	5.1	1.7	c	
	15	36	414	55	454	63	385	49	110	13	62	14.9	3.7	12.3	11.7	5.5	4.4	<LOD	3.5	5.1	<LOD	c	
	18	29	378	43	364	50	318	38	86	11	46	11.4	3.2	10.5	8.8	4.4	3.4	<LOD	3.4	4.2	1.4	c	
	23	46	328	55	514	73	396	52	117	14	60	12.7	3.3	12.3	11.8	5.9	4.9	<LOD	4.3	6.0	2.1	c	
	25	41	451	61	507	70	413	57	127	16	65	17.6	4.8	13.7	12.8	6.4	5.0	<LOD	4.0	5.8	1.7	c	
	28	44	410	64	562	77	460	64	133	17	73	16.3	4.6	16.1	13.2	6.7	5.6	<LOD	4.3	6.4	2.0	c	
	34	86	123	84	922	126	673	88	191	22	84	19.5	3.5	16.3	15.8	8.7	8.2	<LOD	7.0	11.6	3.4	c	
	35	78	118	79	870	120	655	88	186	21	91	19.5	3.7	16.2	16.0	8.7	7.5	<LOD	7.3	11.6	3.6	c	
	36	87	127	88	948	132	696	93	201	24	92	20.1	3.7	18.1	17.4	9.3	8.7	<LOD	7.6	12.6	3.8	c	
MFM_T687:10,648 varve yrs BP																							
	9	216	26	14	606	152	31	109	151	10	25	<LOD	<LOD	<LOD	1.8	1.7	2.2	0.4	4.8	21.3	5.5	a	
	16	181	340	15	368	117	538	81	131	10	32	<LOD	<LOD	<LOD	<LOD	<LOD	<LOD	<LOD	4.8	11.8	3.4	a	
	25	200	366	13	411	126	595	79	123	9	27	<LOD	<LOD	<LOD	2.0	1.2	1.6	0.3	4.2	13.1	3.5	a	
	32	267	98	16	981	249	49	111	167	12	30	<LOD	<LOD	3.3	2.2	1.7	2.9	0.5	5.4	34.1	8.0	a	
	34	199	359	15	455	137	527	96	143	11	30	<LOD	1.0	<LOD	2.1	<LOD	<LOD	<LOD	5.3	14.2	3.8	a	
	38	188	374	18	438	144	525	104	159	13	35	<LOD	<LOD	<LOD	2.9	1.8	2.3	0.4	5.9	15.2	3.6	a	
	39	172	454	16	380	129	697	91	143	11	34	<LOD	0.9	<LOD	2.3	1.6	<LOD	<LOD	5.0	13.3	3.2	a	
	44	224	23	12	537	126	19	97	131	9	22	<LOD	<LOD	<LOD	1.7	1.4	1.8	<LOD	4.2	19.2	5.3	a	
	45	189	97	22	309	147	119	128	218	18	55	6.6	1.0	4.6	3.7	2.2	2.4	0.3	7.2	9.7	2.2	a	
	46	207	252	26	386	110	227	95	155	13	43	6.4	<LOD	<LOD	4.4	2.5	2.8	0.5	4.7	18.8	3.9	a	
	49	90	128	89	956	132	716	96	207	22	93	20.3	4.0	18.6	17.3	9.1	9.0	1.2	7.4	12.4	4.0	b	
	50	89	122	87	873	126	660	86	193	21	83	19.1	3.7	15.3	15.7	8.3	7.8	1.1	6.9	10.6	3.2	b	
	51	83	141	89	923	126	725	93	196	23	96	20.5	4.2	18.2	16.3	8.9	8.1	1.2	7.6	12.2	3.9	a	
		EPMA #	Rb	Sr	Y	Zr	Nb	Ba	La	Ce	Pr	Nd	Sm	Eu	Gd	Dy	Er	Yb	Lu	Ta	Th	U	Std filed
MFM_T685: 10,619 varve yrs BP																							
	6	195	438	15	411	132	798	88	140	11	34	4.7	1.2	<LOD	2.6	1.5	2.0	0.3	5.3	13.8	3.7	d	
	10	197	394	14	374	124	664	89	137	11	31	4.0	1.0	<LOD	2.2	1.6	1.8	0.3	4.7	13.3	3.5	d	
	15	218	280	20	398	154	426	110	176	15	45	5.1	1.3	<LOD	3.1	2.2	2.3	0.4	7.3	13.5	2.8	d	
	16	212	375	15	437	143	584	100	148	12	33	4.0	1.0	<LOD	2.4	1.7	2.0	0.3	5.8	16.3	4.1	d	
	17	242	118	32	563	235	168	145	254	22	67	7.8	1.3	5.8	5.3	3.5	4.1	0.6	10.4	19.3	4.7	d	
	20	192	377	18	348	107	587	88	140	11	34	5.0	1.0	<LOD	2.6	1.9	2.3	0.3	4.3	14.4	3.4	d	
MFM_T573: 7,744 varve yrs BP																							
	2	209	400	15	437	134	653	97	146	11	32	<LOD	1.1	<LOD	2.3	1.5	2.0	<LOD	5.3	16.0	3.8	b	
	3	194	197	12	493	136	166	102	140	10	25	<LOD	<LOD	<LOD	1.8	1.4	2.0	<LOD	4.6	16.9	4.5	b	
	4	190	200	13	498	140	178	102	145	10	24	<LOD	0.6	<LOD	1.8	1.4	2.2	0.3	4.8	17.6	4.6	d	
	6	218	310	11	424	118	542	86	124	9	21	<LOD	0.7	<LOD	1.6	1.3	1.7	0.3	4.1	14.6	4.1	b	
	11	89	121	86	876	130	654	86	192	22	85	18.9	3.5	16.1	15.7	8.2	8.7	1.0	6.5	11.7	3.3	b	
	13	216	325	14	30	11	349	22	43	5	18	3.9	1.0	2.7	2.6	1.4	1.0	<LOD	0.5	3.9	1.0	d	
MFM_T334: 3,382 varve yrs BP																							
	1	94	130	30	448	87	974	65	123	13	47	8.6	2.4	6.7	5.5	3.3	3.2	0.5	4.8	8.2	2.3	a	
	2	134	50	49	881	158	279	99	185	19	59	11.1	1.2	8.3	8.6	5.0	5.9	0.8	8.7	13.3	4.8	a	



595 Table 3:  
 596 Mean varve ages of the main Lateglacial tephra layers and the UMT and their age  
 597 relationships to the major biostratigraphic units (pollen zones) as defined by Litt and Stebich  
 598 (1999) in the MFM sediment record. \*Varve ages from the re-counted interval of the  
 599 MFM2015 varve chronology. For comparison with the GRIP/NGRIP ice cores the Meiendorf  
 600 pollen zone has been tentatively correlated with GI-1e and the Oldest Dryas with GI-1d,  
 601 respectively (Brauer et al., 2000b).

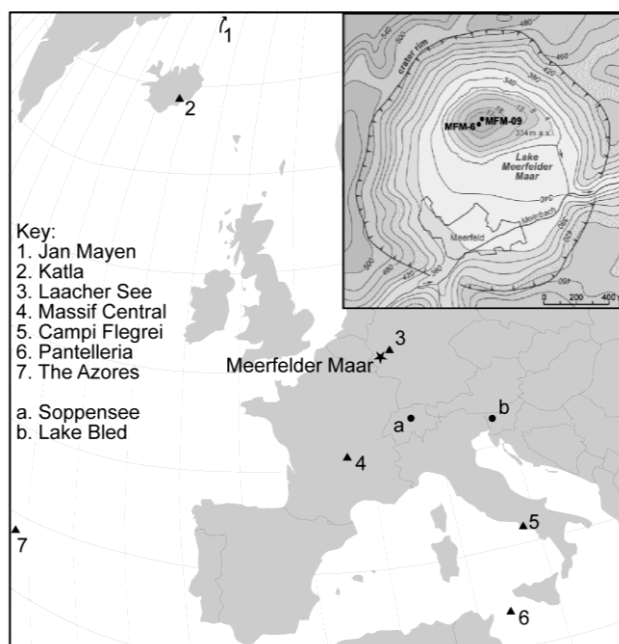
Tephra layer	Boundary	Varve ages BP	Local biostratigraphic position
MFM_T711 / Ulmener Maar tephra, West Eifel, Germany		11,000	590 years after transition to Holocene
	Younger Dryas / Holocene	11,590	
MFM_T801 / Vedde Ash, Katla, Iceland		12,140	539 years after transition to YD; 550 years before transition to Holocene
	Allerød / Younger Dryas	12,679	
MFM_T876 / Laacher See Tephra, East Eifel, Germany		12,880	470 years after start of Allerød; 200 years before transition to YD;
	Meiendorf / Oldest Dryas	13,995*	
MFM_T1072 / Neapolitan Yellow Tuff, Campi Flegrei, Ita		14,230*	350 - 400 years after start of Meiendorf 235 years before transition to Oldest Dryas
	Pleniglacial / Meiendorf	ca. 14,600*	duration extrapolated (no varve counting)

602

603

604

605 Figure 1:  
 606 Location map showing Meerfelder Maar, in the West Eifel, volcanic centres and other sites  
 607 mentioned in the text. Insert shows topography of the Meerfelder crater and bathymetry of  
 608 the lake basin, with the MFM-09 and MFM-6 core locations.

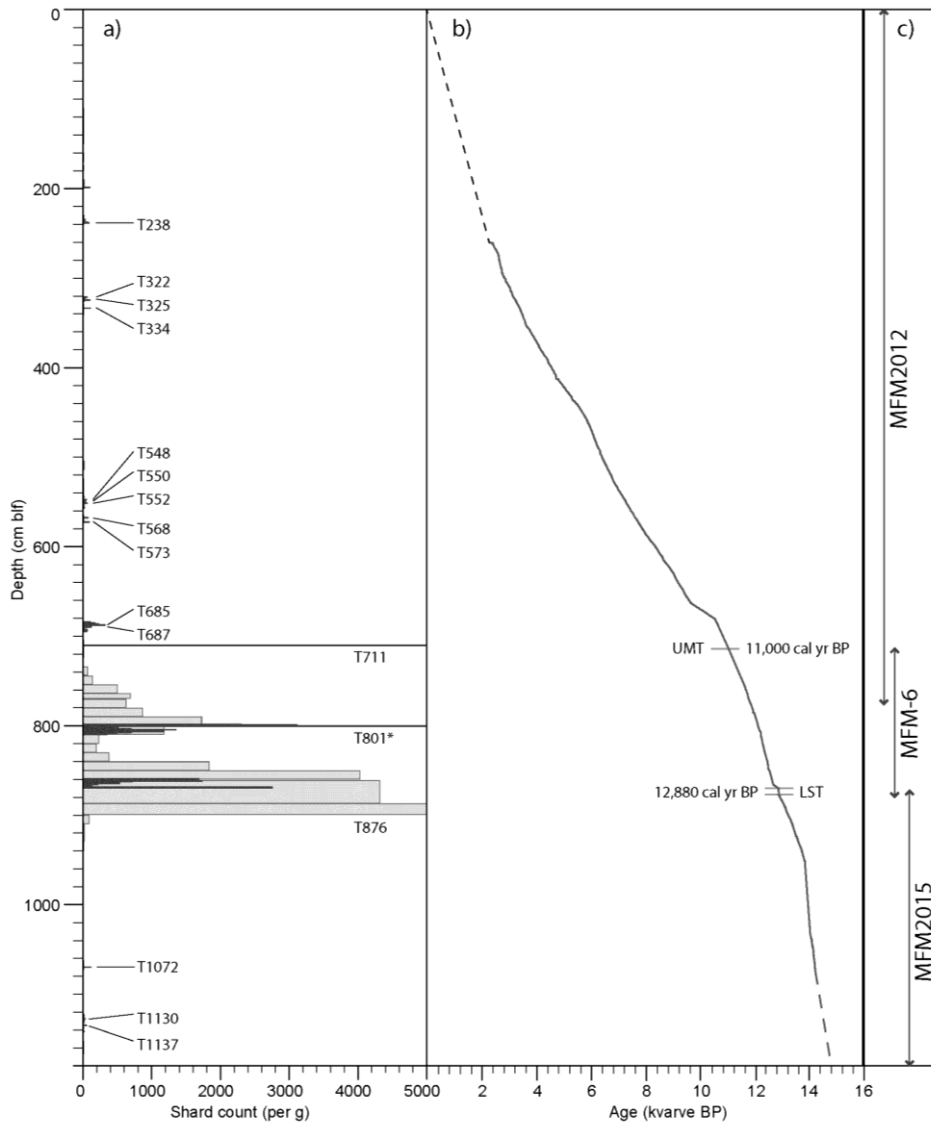


609

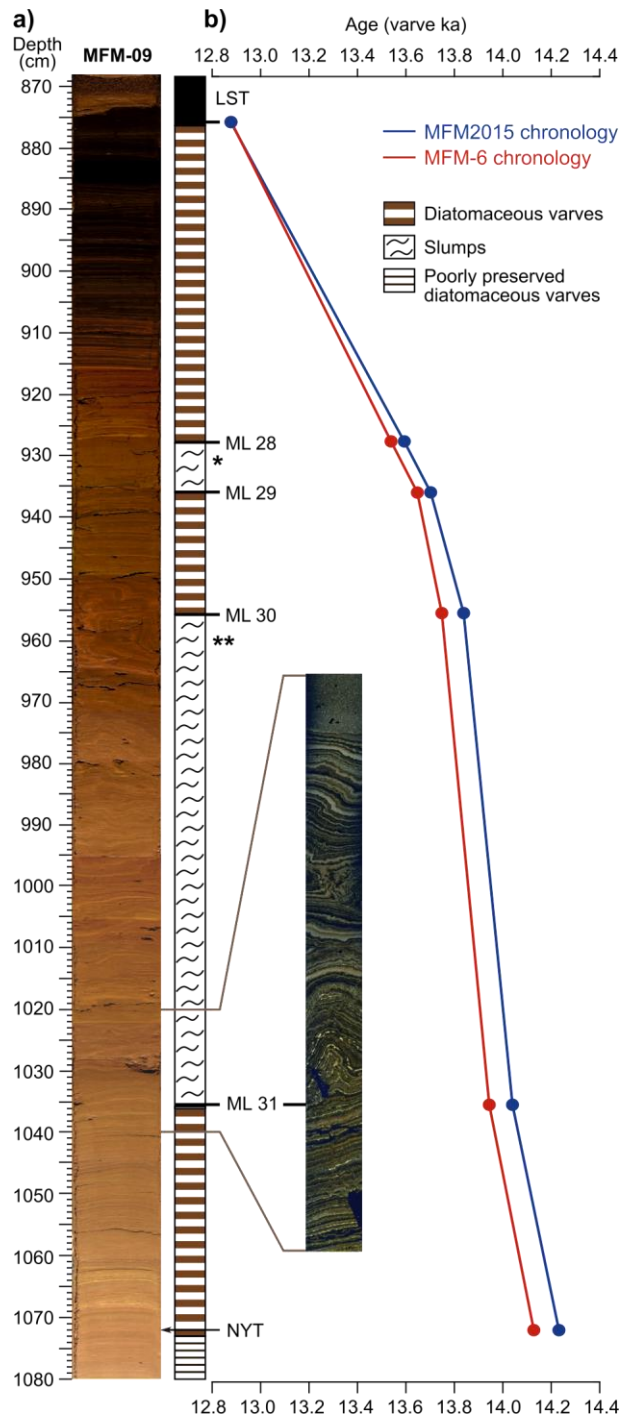
610

611

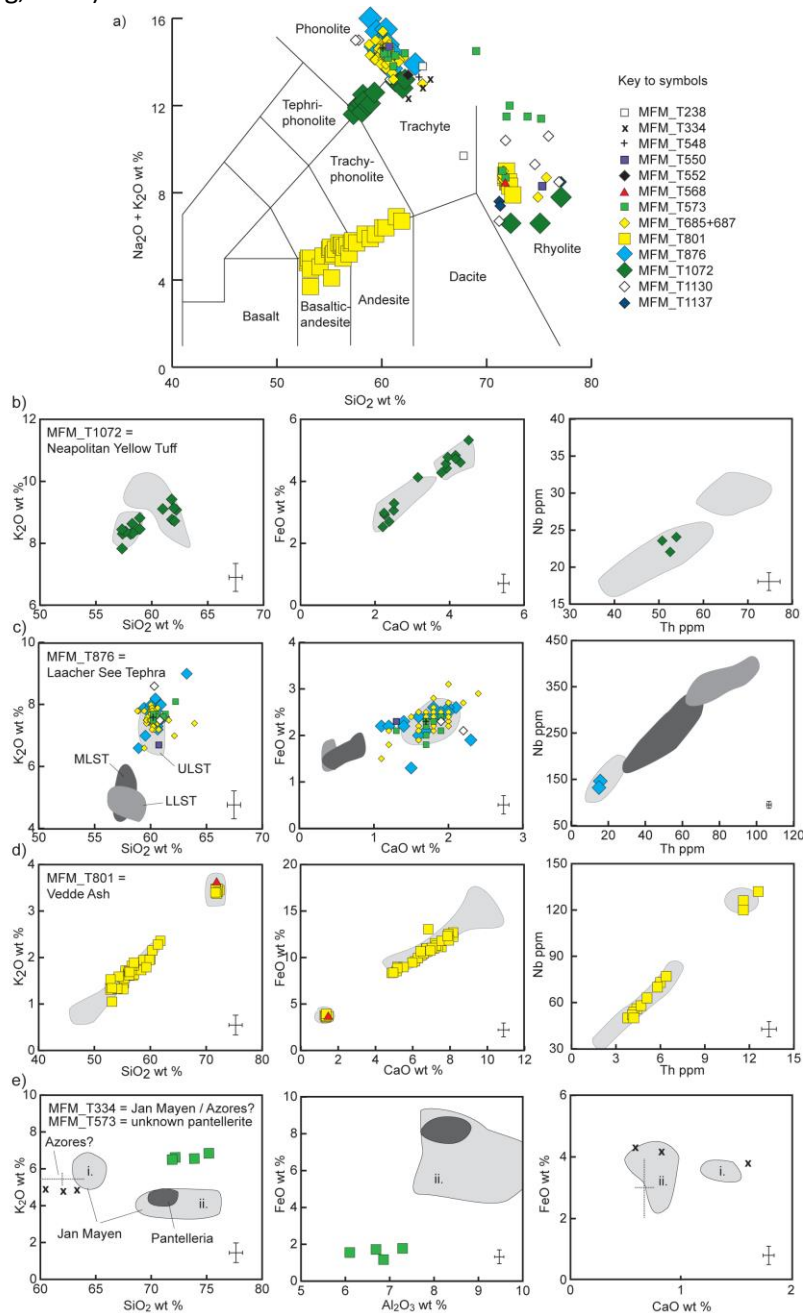
612 Figure 2:  
 613 a) Plot of tephra glass shard counts (shards per gram dry sediment) against MFM09  
 614 composite depth (left hand axis) in the Meerfelder Maar composite profile. Tephra layers  
 615 sample codes are based upon their first occurrence depth below lake floor (cm). b) the  
 616 MFM2015 age-depth profile for MFM09 is shown with the LST and UMT marker tephra  
 617 layers indicated alongside (c) the varve counted sections from the previous MFM cores that  
 618 comprise the final MFM2015 chronology (section 3.1).  
 619



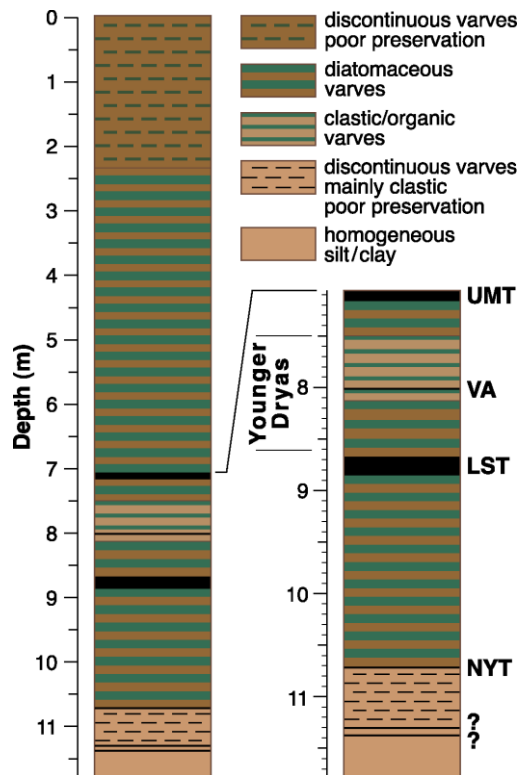
621 Figure 3:  
 622 Core photograph of the section below the Laacher See Tephra (LST) for which the published  
 623 MFM-6 chronology (red line; Brauer et al., 1999) has been slightly revised by varve counting  
 624 in new cores (MFM09), labelled as updated MFM2015 chronology (blue line). (a) Core photo  
 625 and lithological description. (b) Age-depth model for the MFM-6 (in red) and MFM2015 (in  
 626 blue) chronologies. The upper slumped section (\*, 8 cm thick) is present in both composite  
 627 profiles and 110 varves have been interpolated (Brauer et al., 1999). The lower slumped  
 628 section (\*\*, 80 cm thick) is well laminated in the profile MFM-6 and 200 varves have been  
 629 adopted from the MFM-6 chronology. Both records are precisely correlated using four  
 630 macroscopically visible (ML28 – ML31) and microscopic (not shown) marker layers. The  
 631 position of the non-visible Neapolitan Yellow Tuff (NYT) is indicated with an arrow in the  
 632 lower part.  
 633



635 Figure 4:  
 636 Selected bi-plots showing tephra glass shard major, minor and trace element compositions. (a) The  
 637 full dataset from the analysed tephra layers in Meerfelder Maar, plotted using the Total Alkali Silica  
 638 classification by Le Bas et al. (1986). (b) The correlation of the trachytic-phonolitic shards from  
 639 MFM\_T1067 to the Neapolitan Yellow Tuff (data from Tomlinson et al., 2012). (c) MFM\_T876  
 640 correlated to the Laacher See Tephra (proximal glass data from the RESET database, (Bronk Ramsey  
 641 et al., in press-b). Also plotted are other layers containing reworked LST-like tephra (MFM\_T548;  
 642 MFM\_T550; MFM\_T685/687; MFM\_T573; MFM\_T876; MFM\_T1130). A reduced dataset is plotted  
 643 for MFM\_T685+687 for clarity. (d) MFM\_T801 correlated to the Vedde Ash (composite of data from  
 644 Lane et al., 2012b); MFM\_T568 is compositionally indistinguishable on major elements. Error bar  
 645 insets show approximate 2 sigma uncertainty range, based on precision of secondary standard glass  
 646 analyses (supplementary information table 1). (e) Comparison of MFM\_T334 to Holocene trachytic  
 647 tephra from Western Ireland correlated to Jan Mayen (*i.*) and Mt Furnas in the Azores (Chambers et  
 648 al., 2004; Reilly and Mitchell, 2014; Johannesson, in press) and MFM\_T573 to published pantelleritic  
 649 tephra correlated to eruptions of Pantelleria (Magny et al., 2011) and Jan Mayen (*ii.*) (Lacasse and  
 650 Garbe-Schönberg, 2001) .

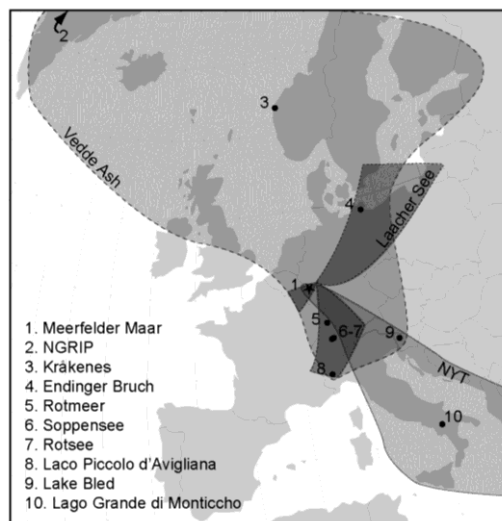


652 Figure 5:  
 653 Lithological profile and summary of the Lateglacial and early Holocene tephrostratigraphy of  
 654 Lake Meerfelder Maar, from the Ulmener Maar tephra to the onset of varve formation in  
 655 MFM09 sequence.



656

657 Figure 6:  
 658 Map showing the known distributions of tephra from the Neapolitan Yellow tuff (Lane et al.,  
 659 2011a and references therein), the Laacher See Tephra (Riede et al., 2011 and references  
 660 therein), and the Vedde Ash (Lane et al., 2012b and references therein). Key sites, and those  
 661 where the tephra layers are co-located, are numbered: 1. Meerfelder Maar, 2. NGRIP  
 662 (Mortensen et al., 2005); 3. Kråkenes (Mangerud et al., 1984); 4. Enderinger Bruch (Lane et al.,  
 663 2012c); 5. Rotmeer; 6. Soppensee; 7. Rotsee; 8. Lago Piccolo di Avigliana (Lane et al., 2012a);  
 664 9. Lake Bled (Lane et al., 2011a); 10. Lago Grande di Monticchio (Wulf et al., 2004).



665

666 Supplementary information:

667 Table S1:

668 Complete datasets of single-shard major and minor element oxide compositions for all  
 669 tephra layers analysed within the Meerfelder Maar record, measured by electron  
 670 microprobe (section 2.3). Data are presented normalised to water-free compositions, with  
 671 original totals shown, after filtering points with analytical totals below 94 weight %.  
 672 Secondary standard data, which provide a measure of precision and accuracy, are presented  
 673 within Supplementary Information (Table S2).

	EPMA #	SiO <sub>2</sub>	TiO <sub>2</sub>	Al <sub>2</sub> O <sub>3</sub>	FeO	MnO	MgO	CaO	Na <sub>2</sub> O	K <sub>2</sub> O	P <sub>2</sub> O <sub>5</sub>	Total	Std file
MFM_T1137	1	71.82	0.02	13.93	3.53	0.19	1.61	2.28	2.70	3.91	0.00	96.79	a
MFM_T1137	2	71.20	0.23	14.94	3.22	0.09	1.01	1.75	3.90	3.67	0.01	99.08	a
MFM_T1137	3	71.27	0.37	14.91	3.12	0.07	1.04	1.77	3.91	3.51	0.02	99.24	e
MFM_T1137	4	77.09	0.06	12.71	1.05	0.01	0.03	0.56	3.79	4.70	0.00	94.42	e
		SiO <sub>2</sub>	TiO <sub>2</sub>	Al <sub>2</sub> O <sub>3</sub>	FeO	MnO	MgO	CaO	Na <sub>2</sub> O	K <sub>2</sub> O	P <sub>2</sub> O <sub>5</sub>	Total	Std file
MFM_T1130	1	57.81	0.33	20.14	2.36	0.17	0.67	3.49	6.18	8.81	0.05	96.77	f
MFM_T1130	2	57.46	0.43	20.00	2.62	0.14	0.94	3.38	6.11	8.92	0.00	97.49	a
MFM_T1130	3	60.28	0.61	20.46	2.35	0.24	0.32	1.94	5.09	8.58	0.13	96.22	a
MFM_T1130	4	60.79	0.57	20.66	2.06	0.14	0.27	2.17	5.77	7.46	0.10	99.53	a
MFM_T1130	5	71.83	0.62	11.53	4.04	0.05	1.21	0.25	2.82	7.61	0.04	95.60	f
MFM_T1130	6	71.17	0.45	13.14	4.19	0.14	1.52	2.61	2.67	4.04	0.08	98.05	g
MFM_T1130	8	74.60	0.12	12.17	2.15	0.01	0.81	0.89	2.55	6.70	0.01	95.50	g
MFM_T1130	9	76.89	0.04	12.88	0.90	0.13	0.04	0.59	3.84	4.64	0.03	95.19	f
		SiO <sub>2</sub>	TiO <sub>2</sub>	Al <sub>2</sub> O <sub>3</sub>	FeO	MnO	MgO	CaO	Na <sub>2</sub> O	K <sub>2</sub> O	P <sub>2</sub> O <sub>5</sub>	Total	Std file
MFM_T1072	1	57.34	0.61	18.67	5.33	0.10	1.50	4.51	3.80	7.83	0.30	94.91	f
MFM_T1072	2	57.67	0.55	19.12	4.76	0.05	1.36	4.19	3.51	8.50	0.31	95.46	e
MFM_T1072	3	57.71	0.59	19.18	4.72	0.04	1.30	4.24	3.53	8.36	0.32	97.62	e
MFM_T1072	4	57.98	0.50	18.87	4.63	0.01	1.24	4.31	3.70	8.43	0.32	97.36	e
MFM_T1072	5	58.10	0.58	18.80	4.84	0.11	1.37	4.16	3.44	8.30	0.31	96.23	a
MFM_T1072	6	58.25	0.54	18.66	4.57	0.17	1.22	3.90	3.83	8.63	0.23	95.92	f
MFM_T1072	7	58.30	0.59	18.66	4.78	0.13	1.17	3.95	3.82	8.33	0.28	94.12	f
MFM_T1072	8	58.72	0.64	18.75	4.42	0.11	1.21	3.92	3.50	8.46	0.28	96.72	a
MFM_T1072	9	58.93	0.48	18.92	4.28	0.14	1.13	3.78	3.59	8.46	0.29	97.74	a
MFM_T1072	10	59.29	0.48	19.14	4.15	0.06	0.94	3.17	3.69	8.87	0.20	94.72	e
MFM_T1072	11	61.35	0.42	18.51	3.31	0.10	0.62	2.52	3.91	9.16	0.11	94.51	e
MFM_T1072	12	61.78	0.40	18.56	3.06	0.14	0.54	2.50	3.52	9.42	0.08	97.63	a
MFM_T1072	13	61.80	0.49	18.76	2.92	0.18	0.44	2.26	4.29	8.77	0.10	97.28	a
MFM_T1072	14	61.98	0.40	18.77	2.70	0.06	0.47	2.38	3.99	9.14	0.10	95.49	f
MFM_T1072	15	62.02	0.43	18.80	2.98	0.22	0.40	2.24	4.10	8.72	0.09	96.88	f
MFM_T1072	16	62.19	0.39	18.91	2.53	0.12	0.41	2.21	4.09	9.08	0.08	95.62	a
MFM_T1072	17	75.14	0.15	14.16	1.74	0.05	0.76	1.15	2.44	4.13	0.29	96.60	f
MFM_T1072	18	72.34	0.59	12.92	3.64	0.24	1.98	1.68	3.20	3.38	0.02	99.46	f
MFM_T1072	19	77.08	0.14	11.82	2.38	0.08	0.02	0.69	4.41	3.38	0.01	96.26	f
		SiO <sub>2</sub>	TiO <sub>2</sub>	Al <sub>2</sub> O <sub>3</sub>	FeO	MnO	MgO	CaO	Na <sub>2</sub> O	K <sub>2</sub> O	P <sub>2</sub> O <sub>5</sub>	Total	Std file
MFM_T876	1	58.91	0.29	21.21	2.22	0.11	0.18	1.09	9.33	6.64	0.03	97.19	e
MFM_T876	2	59.35	0.68	19.97	2.55	0.05	0.47	2.11	6.78	7.91	0.12	96.16	e
MFM_T876	3	59.49	0.37	20.74	2.26	0.10	0.20	1.40	8.44	6.96	0.04	97.36	e
MFM_T876	4	59.71	0.64	20.05	2.61	0.02	0.30	1.83	6.96	7.85	0.04	98.52	e
MFM_T876	5	59.72	0.57	20.34	2.56	0.08	0.24	1.96	6.70	7.78	0.06	98.51	e
MFM_T876	6	59.84	0.45	20.49	1.91	0.11	0.30	2.27	6.80	7.52	0.31	95.41	e
MFM_T876	7	59.88	0.58	20.08	2.45	0.09	0.30	1.93	6.68	7.90	0.10	96.06	e
MFM_T876	8	60.01	0.66	19.69	2.46	0.01	0.34	1.93	6.85	7.96	0.08	95.44	e
MFM_T876	9	60.41	0.57	20.05	2.36	0.11	0.28	1.75	6.73	7.70	0.05	98.36	b
MFM_T876	10	60.44	0.42	19.98	2.17	0.08	0.19	1.22	7.28	8.17	0.04	97.29	e
MFM_T876	11	60.53	0.57	20.02	2.08	0.09	0.25	1.71	6.86	7.82	0.08	97.31	e
MFM_T876	12	60.54	0.61	19.82	2.45	0.20	0.28	1.79	6.41	7.81	0.09	97.55	b
MFM_T876	13	60.56	0.40	20.18	2.36	0.07	0.25	1.74	6.95	7.43	0.05	98.20	e
MFM_T876	14	60.59	0.57	20.01	2.58	0.04	0.28	1.76	6.80	7.32	0.05	97.61	e
MFM_T876	15	60.60	0.57	20.16	2.24	0.06	0.16	1.37	7.57	7.20	0.08	96.85	e
MFM_T876	16	60.62	0.52	20.03	2.40	0.18	0.28	1.56	6.71	7.60	0.10	98.20	b
MFM_T876	17	60.86	0.55	19.78	2.49	0.22	0.27	2.03	5.75	7.98	0.08	96.22	b
MFM_T876	18	61.18	0.48	19.89	2.03	0.16	0.27	1.61	6.74	7.57	0.06	98.59	b
MFM_T876	19	63.19	0.33	19.62	1.26	0.07	0.12	1.49	4.87	9.03	0.03	99.07	b

674

		SiO <sub>2</sub>	TiO <sub>2</sub>	Al <sub>2</sub> O <sub>3</sub>	FeO	MnO	MgO	CaO	Na <sub>2</sub> O	K <sub>2</sub> O	P <sub>2</sub> O <sub>5</sub>	Total	Std file
MFM_T801	1	52.88	3.58	13.61	12.26	0.21	3.93	8.18	3.45	1.36	0.54	96.93	c
MFM_T801	2	52.90	3.59	13.50	12.54	0.20	3.95	7.91	3.61	1.31	0.49	96.65	c
MFM_T801	3	52.96	5.15	12.95	13.06	0.24	3.45	6.84	3.44	1.53	0.38	96.03	c
MFM_T801	4	53.16	3.55	13.57	12.32	0.23	3.90	7.87	3.62	1.34	0.43	96.64	c
MFM_T801	5	53.21	3.44	13.47	12.70	0.28	3.81	8.17	3.15	1.32	0.46	97.52	c
MFM_T801	6	53.22	2.84	10.70	11.80	0.20	7.17	10.06	2.63	1.05	0.33	98.06	c
MFM_T801	7	54.14	3.45	13.46	11.85	0.28	3.83	7.95	3.23	1.33	0.48	96.25	c
MFM_T801	8	54.43	3.12	13.77	11.81	0.20	3.58	7.55	3.49	1.59	0.46	96.73	c
MFM_T801	9	55.01	3.23	13.52	11.54	0.19	3.50	7.20	3.81	1.57	0.43	98.42	c
MFM_T801	10	55.05	3.18	13.69	11.14	0.13	3.47	7.36	3.96	1.58	0.43	98.25	c
MFM_T801	11	55.20	2.13	10.85	10.11	0.37	6.50	10.46	2.77	1.33	0.29	97.54	c
MFM_T801	12	55.32	3.26	13.12	11.14	0.18	3.92	7.55	3.66	1.46	0.40	95.01	d
MFM_T801	13	55.39	3.17	13.64	11.28	0.15	3.49	7.27	3.61	1.56	0.44	97.23	c
MFM_T801	14	55.62	2.98	13.81	10.97	0.22	3.44	7.15	3.72	1.72	0.38	97.27	c
MFM_T801	15	55.95	2.80	14.14	10.63	0.30	3.07	6.78	3.99	1.72	0.64	97.97	c
MFM_T801	16	56.08	2.81	13.96	10.79	0.25	3.19	6.82	3.92	1.65	0.52	97.79	c
MFM_T801	17	56.18	3.00	13.51	10.98	0.30	3.27	6.74	3.89	1.71	0.43	97.50	c
MFM_T801	18	56.34	2.95	13.73	11.05	0.28	3.21	7.05	3.39	1.62	0.37	93.38	c
MFM_T801	19	56.35	2.84	13.56	10.75	0.21	3.37	6.95	3.83	1.69	0.45	98.19	c
MFM_T801	20	56.72	2.69	13.54	10.97	0.22	3.11	6.71	3.82	1.82	0.38	97.89	c
MFM_T801	21	56.93	2.88	13.36	10.92	0.12	3.29	6.95	3.60	1.61	0.34	97.68	d
MFM_T801	22	57.12	2.68	14.13	10.26	0.16	2.89	6.50	4.07	1.64	0.55	98.51	c
MFM_T801	23	57.21	2.61	13.65	10.50	0.16	3.13	6.59	3.96	1.83	0.37	97.28	c
MFM_T801	24	57.62	2.51	14.17	9.95	0.28	2.83	6.28	4.02	1.73	0.62	95.58	c
MFM_T801	25	58.43	2.25	14.30	9.48	0.19	2.60	5.98	4.38	1.73	0.67	98.30	c
MFM_T801	26	58.86	2.42	13.50	9.60	0.18	3.05	6.13	3.94	1.95	0.37	96.83	c
MFM_T801	27	59.35	2.08	14.57	8.98	0.29	2.38	5.51	4.33	1.79	0.70	98.22	c
MFM_T801	28	60.07	1.91	14.40	9.00	0.26	2.24	5.18	4.39	1.97	0.58	97.66	c
MFM_T801	29	60.39	0.60	20.17	2.26	0.09	0.29	1.82	6.50	7.83	0.06	97.02	c
MFM_T801	30	60.42	2.13	14.28	8.88	0.23	2.10	5.18	4.25	2.15	0.38	97.40	c
MFM_T801	31	61.44	1.81	13.81	8.37	0.19	2.17	4.95	4.64	2.28	0.35	98.67	c
MFM_T801	32	61.88	1.66	13.96	8.35	0.17	2.08	4.87	4.34	2.36	0.33	97.51	c
MFM_T801	34	71.78	0.34	13.39	3.95	0.14	0.22	1.36	5.34	3.40	0.08	97.05	d
MFM_T801	35	71.85	0.29	13.43	3.68	0.20	0.20	1.47	5.35	3.47	0.06	95.58	d
MFM_T801	36	71.86	0.28	13.56	3.55	0.17	0.19	1.34	5.51	3.48	0.05	98.62	d
MFM_T801	37	72.01	0.34	13.71	3.71	0.17	0.18	1.36	5.09	3.37	0.06	99.20	d
MFM_T801	38	72.15	0.27	13.60	3.68	0.18	0.20	1.43	5.00	3.49	0.01	98.22	d
MFM_T801	39	72.25	0.34	13.76	3.65	0.13	0.20	1.30	4.87	3.42	0.07	94.40	d
MFM_T801	40	72.50	0.28	13.79	3.80	0.18	0.21	1.28	4.49	3.46	0.03	96.67	d
		SiO <sub>2</sub>	TiO <sub>2</sub>	Al <sub>2</sub> O <sub>3</sub>	FeO	MnO	MgO	CaO	Na <sub>2</sub> O	K <sub>2</sub> O	P <sub>2</sub> O <sub>5</sub>	Total	Std file
MFM_T687	1	58.90	0.92	20.10	2.87	0.03	0.33	2.42	6.54	7.78	0.12	96.57	e
MFM_T687	2	59.86	0.58	20.22	2.42	0.10	0.32	1.88	6.89	7.64	0.09	95.85	c
MFM_T687	3	59.82	0.63	20.10	2.24	0.14	0.31	1.75	7.37	7.57	0.07	96.51	c
MFM_T687	4	60.21	0.60	20.28	2.49	0.05	0.28	1.91	6.42	7.70	0.06	96.19	e
MFM_T687	5	60.13	0.60	20.16	2.35	0.04	0.32	1.87	6.59	7.88	0.07	96.41	e
MFM_T687	6	59.96	0.62	20.44	2.36	0.08	0.30	1.95	6.37	7.88	0.05	96.73	e
MFM_T687	7	58.76	0.87	19.88	3.08	0.06	0.45	1.95	7.06	7.78	0.11	98.75	e
MFM_T687	8	59.67	0.62	20.03	2.56	0.06	0.29	2.04	6.96	7.50	0.27	97.29	e
MFM_T687	9	59.43	0.37	21.23	1.92	0.21	0.15	1.60	8.46	6.56	0.06	97.78	a
MFM_T687	10	60.01	0.63	19.99	2.27	0.02	0.32	1.97	6.68	8.05	0.07	96.88	e
MFM_T687	11	60.05	0.63	20.03	2.30	0.06	0.32	2.06	5.43	8.95	0.18	97.00	e
MFM_T687	12	60.07	0.60	20.51	2.30	0.06	0.32	1.83	6.79	7.43	0.09	97.09	e
MFM_T687	13	60.28	0.57	20.05	2.50	0.21	0.32	1.75	7.02	7.23	0.07	96.86	a
MFM_T687	14	60.11	0.49	20.23	2.36	0.08	0.30	1.84	6.85	7.69	0.05	97.21	e
MFM_T687	15	60.31	0.63	20.30	2.42	0.12	0.30	1.81	6.39	7.64	0.07	96.99	a
MFM_T687	16	60.25	0.58	20.38	2.48	0.15	0.32	1.86	6.54	7.37	0.08	97.17	a
MFM_T687	17	59.27	0.74	20.01	2.90	0.17	0.44	2.26	6.88	7.23	0.10	98.78	a

MFM_T687	18	59.88	0.55	20.14	2.52	0.04	0.33	1.85	7.02	7.59	0.08	97.84	e
MFM_T687	19	59.70	0.58	20.50	2.40	0.09	0.25	1.83	6.97	7.62	0.06	98.22	e
MFM_T687	20	60.06	0.56	20.26	2.48	0.09	0.34	1.92	6.38	7.83	0.07	97.75	e
MFM_T687	21	59.86	0.55	20.44	2.20	0.15	0.27	2.00	6.61	7.84	0.08	98.08	a
MFM_T687	22	60.04	0.58	20.19	2.55	0.05	0.33	1.84	6.62	7.76	0.04	97.84	e
MFM_T687	23	60.25	0.57	20.42	2.29	0.11	0.33	1.87	6.53	7.49	0.14	97.58	a
MFM_T687	24	60.23	0.62	19.70	2.51	0.13	0.36	2.03	7.01	7.33	0.09	97.67	e
MFM_T687	25	60.56	0.46	20.39	2.21	0.16	0.28	1.61	6.62	7.65	0.05	97.20	a
MFM_T687	26	60.39	0.51	20.46	2.21	0.10	0.28	1.75	6.75	7.47	0.07	97.50	a
MFM_T687	27	60.12	0.29	20.78	1.84	0.13	0.15	1.24	8.24	7.18	0.02	97.93	e
MFM_T687	28	60.15	0.56	20.18	2.46	0.07	0.29	1.85	6.73	7.67	0.05	97.93	e
MFM_T687	29	60.45	0.48	20.23	2.08	0.12	0.28	1.81	6.59	7.90	0.07	97.49	e
MFM_T687	30	60.13	0.50	20.26	2.23	0.10	0.31	1.83	6.64	7.94	0.08	98.14	e
MFM_T687	31	60.28	0.47	20.42	2.12	0.07	0.24	1.60	6.94	7.81	0.05	98.05	e
MFM_T687	32	60.14	0.60	19.87	2.62	0.25	0.30	2.01	6.95	7.16	0.10	98.30	a
MFM_T687	33	60.37	0.54	20.53	2.23	0.00	0.30	1.72	6.66	7.60	0.06	97.95	e
MFM_T687	34	60.21	0.48	20.37	2.27	0.15	0.29	1.82	6.74	7.59	0.08	98.21	a
MFM_T687	35	60.50	0.34	20.63	1.85	0.08	0.15	1.42	7.29	7.68	0.06	97.84	e
MFM_T687	36	60.19	0.55	20.29	2.25	0.17	0.25	1.82	6.78	7.62	0.09	98.38	a
MFM_T687	37	60.35	0.51	20.13	2.11	0.19	0.30	1.79	6.77	7.72	0.11	98.24	a
MFM_T687	38	60.18	0.61	20.03	2.30	0.15	0.33	1.88	6.59	7.86	0.08	98.87	a
MFM_T687	39	60.01	0.57	20.20	2.23	0.18	0.37	2.01	6.63	7.75	0.07	99.22	a
MFM_T687	40	60.56	0.68	19.35	2.75	0.22	0.35	1.80	6.73	7.45	0.09	98.44	a
MFM_T687	41	60.70	0.23	20.77	1.86	0.21	0.16	1.21	7.77	7.06	0.03	98.56	a
MFM_T687	42	60.69	0.42	20.59	2.12	0.14	0.20	1.20	7.35	7.25	0.04	99.02	a
MFM_T687	43	62.12	0.21	20.49	1.54	0.15	0.15	1.11	7.21	7.00	0.02	97.74	a
MFM_T687	44	61.68	0.33	20.69	1.67	0.15	0.15	1.22	7.13	6.93	0.06	98.46	a
MFM_T687	45	61.60	0.56	19.37	2.09	0.19	0.35	1.78	6.42	7.53	0.10	99.31	a
MFM_T687	46	63.95	0.62	18.02	2.42	0.08	0.31	1.49	5.64	7.37	0.11	98.64	a
MFM_T687	47	71.57	0.30	13.95	3.64	0.19	0.24	1.45	5.10	3.47	0.09	97.26	a
MFM_T687	48	71.64	0.30	13.69	3.78	0.13	0.22	1.35	5.36	3.47	0.05	97.33	a
MFM_T687	49	71.61	0.32	13.54	3.93	0.00	0.19	1.41	5.36	3.59	0.05	97.38	e
MFM_T687	50	71.61	0.31	13.72	3.69	0.04	0.20	1.35	5.43	3.61	0.04	97.96	e
MFM_T687	51	71.45	0.27	13.78	3.95	0.14	0.22	1.34	5.27	3.52	0.06	98.85	a
MFM_T687	52	74.93	0.39	13.69	2.28	0.00	0.47	0.33	2.64	5.20	0.07	94.66	c
		<b>SiO<sub>2</sub></b>	<b>TiO<sub>2</sub></b>	<b>Al<sub>2</sub>O<sub>3</sub></b>	<b>FeO</b>	<b>MnO</b>	<b>MgO</b>	<b>CaO</b>	<b>Na<sub>2</sub>O</b>	<b>K<sub>2</sub>O</b>	<b>P<sub>2</sub>O<sub>5</sub></b>	<b>Total</b>	<b>Std file</b>
MFM_T685	1	60.60	0.60	20.00	2.41	0.13	0.31	2.03	5.90	7.91	0.11	94.55	c
MFM_T685	2	60.16	0.54	19.94	2.33	0.18	0.33	1.86	6.74	7.82	0.09	95.57	c
MFM_T685	3	60.07	0.52	20.09	2.52	0.21	0.28	1.65	6.77	7.79	0.08	95.89	c
MFM_T685	4	59.63	0.68	20.24	2.67	0.19	0.32	1.97	6.85	7.36	0.08	97.16	c
MFM_T685	5	60.48	0.29	20.71	1.96	0.20	0.18	1.42	7.80	6.89	0.07	96.20	a
MFM_T685	6	59.60	0.67	20.18	2.69	0.16	0.35	2.03	6.79	7.46	0.08	97.67	a
MFM_T685	7	59.37	0.63	20.37	2.70	0.14	0.35	2.19	6.29	7.82	0.13	98.25	a
MFM_T685	8	60.34	0.49	20.34	2.17	0.15	0.24	1.65	6.77	7.77	0.07	97.25	c
MFM_T685	9	60.20	0.55	20.30	2.26	0.15	0.29	1.82	6.73	7.65	0.07	97.55	c
MFM_T685	10	60.13	0.56	20.48	2.32	0.20	0.30	1.81	6.67	7.45	0.07	97.77	a
MFM_T685	11	60.41	0.56	20.25	2.17	0.10	0.27	1.87	6.49	7.68	0.18	97.47	a
MFM_T685	12	60.97	0.62	20.04	2.52	0.06	0.30	1.88	6.06	7.46	0.10	96.70	c
MFM_T685	13	60.21	0.60	20.28	2.43	0.18	0.28	1.69	6.82	7.45	0.06	98.19	c
MFM_T685	14	60.38	0.63	20.21	2.48	0.21	0.32	1.97	6.25	7.45	0.10	97.94	c
MFM_T685	15	59.88	0.74	20.16	2.76	0.19	0.44	1.82	6.41	7.49	0.12	99.16	a
MFM_T685	16	59.98	0.53	20.09	2.39	0.27	0.29	1.85	7.04	7.49	0.08	99.01	a
MFM_T685	17	61.13	0.71	19.60	2.80	0.30	0.35	1.87	6.21	6.96	0.08	97.45	a
MFM_T685	18	60.42	0.62	20.31	2.27	0.20	0.31	1.93	6.25	7.62	0.08	98.76	c
MFM_T685	19	60.76	0.41	20.45	2.18	0.14	0.22	1.69	6.59	7.45	0.10	98.33	a
MFM_T685	20	60.59	0.45	20.12	2.18	0.12	0.30	1.85	6.64	7.69	0.06	98.97	a
MFM_T685	21	71.63	0.29	13.62	3.70	0.09	0.26	1.37	5.39	3.61	0.03	98.54	e
MFM_T685	22	71.45	0.27	13.78	3.95	0.14	0.22	1.34	5.27	3.52	0.06	98.85	a
MFM_T685	23	75.70	0.27	13.10	1.66	0.06	0.16	0.23	2.53	6.15	0.13	95.85	a
		<b>SiO<sub>2</sub></b>	<b>TiO<sub>2</sub></b>	<b>Al<sub>2</sub>O<sub>3</sub></b>	<b>FeO</b>	<b>MnO</b>	<b>MgO</b>	<b>CaO</b>	<b>Na<sub>2</sub>O</b>	<b>K<sub>2</sub>O</b>	<b>P<sub>2</sub>O<sub>5</sub></b>	<b>Total</b>	<b>Std file</b>
MFM_T573	1	60.40	0.56	19.81	2.41	0.17	0.31	1.95	6.58	7.72	0.09	97.57	g
MFM_T573	2	60.60	0.55	20.02	2.25	0.20	0.31	1.83	6.60	7.55	0.09	97.45	g
MFM_T573	3	60.48	0.46	20.25	2.21	0.23	0.22	1.69	6.81	7.56	0.08	97.88	g
MFM_T573	4	60.20	0.39	20.39	2.33	0.24	0.23	1.68	6.98	7.53	0.05	98.68	f
MFM_T573	5	60.18	0.47	20.45	2.11	0.17	0.24	1.86	6.73	7.69	0.10	99.33	a
MFM_T573	6	61.29	0.38	20.22	1.77	0.05	0.20	1.72	6.63	7.70	0.04	97.66	g
MFM_T573	7	61.11	0.39	20.52	2.02	0.20	0.21	1.67	6.21	7.60	0.07	98.90	f
MFM_T573	8	62.19	0.33	19.12	2.06	0.13	0.42	1.33	6.26	8.12	0.02	99.28	g
MFM_T573	9	71.81	0.30	13.56	3.76	0.20	0.23	1.36	5.09	3.64	0.06	96.52	g
MFM_T573	10	71.48	0.28	13.50	4.01	0.13	0.21	1.34	5.50	3.50	0.03	97.87	g
MFM_T573	11	69.00	0.69	7.45	4.68	0.11	1.60	1.89	5.93	8.59	0.06	98.65	f
MFM_T573	12	72.21	0.46	7.29	3.38	0.09	1.78	2.71	5.39	6.62	0.08	98.48	g
MFM_T573	13	71.93	0.60	6.69	4.38	0.10	1.72	3.00	5.04	6.51	0.05	98.93	f
MFM_T573	14	73.93	0.18	6.10	3.82	0.08	1.55	2.81	4.95	6.54	0.03	96.86	f
MFM_T573	15	75.25	0.11	6.86	3.00	0.05	1.17	2.17	4.56	6.81	0.02	98.94	g



		SiO <sub>2</sub>	TiO <sub>2</sub>	Al <sub>2</sub> O <sub>3</sub>	FeO	MnO	MgO	CaO	Na <sub>2</sub> O	K <sub>2</sub> O	P <sub>2</sub> O <sub>5</sub>	Total	Std file
MFM T568	1	71.76	0.30	13.96	3.69	0.13	0.21	1.37	4.89	3.63	0.06	98.49	a
		SiO <sub>2</sub>	TiO <sub>2</sub>	Al <sub>2</sub> O <sub>3</sub>	FeO	MnO	MgO	CaO	Na <sub>2</sub> O	K <sub>2</sub> O	P <sub>2</sub> O <sub>5</sub>	Total	Std file
MFM T552	1	62.49	0.64	19.03	2.22	0.24	0.34	1.49	6.40	7.04	0.12	100.33	a
		SiO <sub>2</sub>	TiO <sub>2</sub>	Al <sub>2</sub> O <sub>3</sub>	FeO	MnO	MgO	CaO	Na <sub>2</sub> O	K <sub>2</sub> O	P <sub>2</sub> O <sub>5</sub>	Total	Std file
MFM T550	1	60.68	0.61	19.83	2.30	0.19	0.28	1.34	7.95	6.75	0.08	97.18	f
MFM T550	2	75.26	0.49	13.70	1.33	0.11	0.36	0.46	3.59	4.70	0.02	95.67	f
		SiO <sub>2</sub>	TiO <sub>2</sub>	Al <sub>2</sub> O <sub>3</sub>	FeO	MnO	MgO	CaO	Na <sub>2</sub> O	K <sub>2</sub> O	P <sub>2</sub> O <sub>5</sub>	Total	Std file
MFM T548	1	60.25	0.52	20.10	2.30	0.23	0.25	1.71	7.01	7.58	0.05	98.78	f
MFM T548	2	63.61	0.27	17.96	3.66	0.27	0.19	0.70	7.98	5.31	0.04	98.33	f
		SiO <sub>2</sub>	TiO <sub>2</sub>	Al <sub>2</sub> O <sub>3</sub>	FeO	MnO	MgO	CaO	Na <sub>2</sub> O	K <sub>2</sub> O	P <sub>2</sub> O <sub>5</sub>	Total	Std file
MFM T334	1	62.49	0.64	17.99	3.92	0.21	0.58	1.67	7.30	5.00	0.20	96.73	f
MFM T334	2	63.88	0.41	17.16	4.28	0.24	0.28	0.86	7.95	4.87	0.08	97.18	f
MFM T334	3	64.59	0.21	16.62	4.38	0.22	0.12	0.60	8.33	4.90	0.03	98.00	f
		SiO <sub>2</sub>	TiO <sub>2</sub>	Al <sub>2</sub> O <sub>3</sub>	FeO	MnO	MgO	CaO	Na <sub>2</sub> O	K <sub>2</sub> O	P <sub>2</sub> O <sub>5</sub>	Total	Std file
MFM T239	1	63.87	0.08	19.03	0.96	0.09	0.41	1.78	6.39	7.38	0.01	100.36	a
MFM T239	2	67.85	0.59	14.73	4.68	0.17	1.88	0.25	2.80	6.86	0.18	99.85	a

677

678 Table S2:

679 Summary of measured secondary standard glass ((ATHO-G and StHs6/80-G from the MPI-DING  
680 collection, Jochum et al., 2006) compositions by (a) WDS-EPMA and (b) LA-ICP-MS. Preferred values  
681 from the online GeoREM database are listed for comparison (Jochum et al., 2005).

a) WDS-EPMA												
	SiO <sub>2</sub>	TiO <sub>2</sub>	Al <sub>2</sub> O <sub>3</sub>	FeO	MnO	MgO	CaO	Na <sub>2</sub> O	K <sub>2</sub> O	P <sub>2</sub> O <sub>5</sub>		
<b>Observed values:</b>	wt %											
<b>a. ATHO-g</b>												
average (n=11)	75.02	0.25	12.30	3.28	0.09	0.11	1.70	4.15	2.68	0.03		
2σ	0.47	0.07	0.18	0.21	0.08	0.03	0.07	0.39	0.14	0.04		
<b>a. StHs6/80-g</b>												
average (n=10)	63.07	0.71	17.43	4.36	0.07	1.96	5.22	4.40	1.31	0.15		
2σ	0.71	0.05	0.40	0.25	0.09	0.10	0.12	0.98	0.05	0.04		
<b>b. ATHO-g</b>												
average (n=4)	75.51	0.25	12.15	3.35	0.09	0.10	1.71	4.11	2.65	0.01		
2σ	0.19	0.03	0.29	0.23	0.07	0.02	0.04	0.21	0.09	0.02		
<b>b. StHs6/80-g</b>												
average (n=3)	63.13	0.69	17.59	4.40	0.10	1.90	5.21	4.56	1.31	0.11		
2σ	0.25	0.09	0.25	0.34	0.02	0.05	0.08	0.22	0.07	0.01		
<b>c. ATHO-g</b>												
average (n=19)	75.09	0.25	12.26	3.31	0.11	0.09	1.67	4.04	2.75	0.03		
2σ	0.63	0.05	0.25	0.14	0.05	0.03	0.07	0.20	0.11	0.03		
<b>c. StHs6/80-g</b>												
average (n=17)	63.26	0.70	17.68	4.39	0.08	1.95	5.24	4.51	1.30	0.16		
2σ	0.44	0.08	0.41	0.34	0.07	0.06	0.10	0.32	0.07	0.04		
<b>d. ATHO-g</b>												
average (n=6)	74.74	0.25	12.45	3.24	0.11	0.09	1.67	4.06	2.71	0.02		
2σ	0.81	0.04	0.25	0.24	0.05	0.04	0.08	0.31	0.08	0.04		
<b>d. StHs6/80-g</b>												
average (n=4)	64.07	0.72	17.98	4.27	0.06	1.99	5.26	4.56	1.28	0.15		
2σ	0.48	0.10	0.26	0.43	0.09	0.06	0.10	0.42	0.08	0.02		
<b>e. ATHO-g</b>												
average (n=15)	75.21	0.26	12.38	3.33	0.05	0.10	1.69	4.13	2.74	0.03		
2σ	0.78	0.05	0.22	0.28	0.07	0.03	0.09	0.27	0.11	0.04		
<b>e. StHs6/80-g</b>												
average (n=20)	63.63	0.70	17.84	4.40	0.03	1.95	5.30	4.50	1.31	0.15		
2σ	0.51	0.06	0.35	0.33	0.03	0.07	0.19	0.27	0.08	0.03		
<b>f. ATHO-g</b>												
average (n=16)	75.07	0.26	12.28	3.38	0.11	0.09	1.68	3.99	2.75	0.02		
2σ	0.46	0.04	0.16	0.23	0.07	0.04	0.09	0.36	0.13	0.03		
<b>f. StHs6/80-g</b>												
average (n=14)	63.43	0.72	17.53	4.33	0.08	1.94	5.33	4.45	1.29	0.15		
2σ	0.55	0.06	0.28	0.19	0.08	0.09	0.13	0.24	0.08	0.03		
<b>g. ATHO-g</b>												
average (n=5)	75.34	0.24	12.18	3.27	0.09	0.10	1.67	4.10	2.72	0.02		
2σ	0.29	0.08	0.10	0.28	0.09	0.03	0.07	0.28	0.17	0.02		
<b>g. StHs6/80-g</b>												
average (n=7)	63.64	0.72	17.54	4.35	0.10	1.97	5.30	4.58	1.34	0.16		
2σ	0.42	0.06	0.38	0.21	0.09	0.08	0.14	0.21	0.08	0.04		
<b>Preferred values:</b>												
<b>ATHO-G</b>												
preferred value	75.60	0.26	12.20	3.27	0.11	0.10	1.70	3.75	2.64	0.16		
95% CL	0.70	0.02	0.20	0.10	0.01	0.01	0.03	0.31	0.09	0.02		
<b>StHs6/80-g</b>												
preferred value	63.70	0.70	17.80	4.37	0.08	1.97	5.28	4.44	1.29	0.03		
95% CL	0.50	0.02	0.20	0.07	0.00	0.04	0.09	0.14	0.02	0.00		

682

b) LA-ICP-MS		Rb	Sr	Y	Zr	Nb	Ba	La	Ce	Pr	Nd	Sm	Eu	Gd	Dy	Er	Yb	Ta	Th	U
(ppm)																				
Observed values:																				
a. ATHO-g																				
average (n=3)	67	98	94	511	59	567	56	125	15	62	15	2.6	14.7	16.8	10.3	10.7	3.8	7.4	2.4	
2σ	5.9	9.4	3.2	35.2	6.7	40.6	1.4	8.0	1.2	4.0	2.0	0.2	1.3	0.4	0.9	0.9	0.1	0.4	0.3	
a. StHs6/80-g																				
average (n=3)	30	489	11	117	6	300	12	25	3	13	<LOD	1.0	<LOD	2.2	1.2	<LOD	<LOD	2.3	1.0	
2σ	2.1	10.4	0.9	4.4	0.4	14.0	0.9	0.3	0.1	0.7	<LOD	0.1	<LOD	0.2	0.1	<LOD	<LOD	0.1	0.0	
b. ATHO-g																				
average (n=3)	67	95	91	499	59	553	56	122	14	63	15	2.5	14.2	16.7	10.2	10.4	3.8	7.2	2.2	
2σ	1.8	8.0	7.0	35.6	2.1	26.0	4.2	8.4	0.6	9.8	2.3	0.2	1.3	1.8	0.7	1.3	0.2	1.0	0.2	
b. StHs6/80-g																				
average (n=3)	31	480	11	115	6	297	12	25	3	12	<LOD	0.9	<LOD	2.2	1.4	<LOD	<LOD	2.2	1.4	
2σ	2.5	20.3	0.7	7.7	0.3	10.4	1.1	1.2	0.1	1.3	<LOD	0.0	<LOD	0.1	1.1	<LOD	<LOD	0.2	1.4	
c. ATHO-g																				
average (n=3)	67	96	90	495	60	555	55	123	14	62	15	2.5	14.5	16.4	10.1	10.2	3.8	7.1	2.3	
2σ	7.7	6.5	5.9	39.0	5.3	29.7	2.4	7.8	0.9	2.9	1.9	0.2	0.5	0.9	0.6	0.7	0.3	0.3	0.1	
c. StHs6/80-g																				
average (n=3)	30	471	11	112	7	294	11	25	3	13	3	0.9	3.1	2.2	1.3	1.3	<LOD	2.2	0.9	
2σ	2.7	18.3	0.6	3.9	0.5	7.1	0.6	1.1	0.1	1.3	0.8	0.0	1.3	0.5	0.6	0.3	<LOD	0.3	0.0	
d. ATHO-g																				
average (n=3)	68.1	99.3	93.8	507.3	61.3	575.2	57.0	125.4	14.7	62.9	14	2.8	14.4	16.4	10.5	10.6	3.9	7.6	2.3	
2σ	3.0	2.0	3.0	20.5	1.6	6.4	1.3	2.5	0.5	1.2	2.1	0.1	0.3	0.6	0.6	0.5	0.1	0.3	0.1	
d. StHs6/80-g																				
average (n=3)	31.8	485.0	11.0	115.5	6.6	301.0	11.9	25.6	3.0	12.8	<LOD	0.9	2.8	2.1	1.2	1.2	0.5	2.2	1.0	
2σ	1.0	10.8	0.4	2.8	0.5	2.5	0.3	0.8	0.2	1.3	<LOD	0.0	0.6	0.2	0.1	0.1	0.0	0.2	0.0	
Preferred values:																				
Atho-G	65	94	95	512	62	547	56	121	15	61	14	2.8	15.3	16.2	10.3	10.5	3.9	7.4	2.4	
StHs6/80-G	31	482	11.4	118.0	6.9	298.0	12.0	26.1	3.2	13.0	2.8	1.0	2.6	2.2	1.2	1.1	0.4	2.3	1.0	

683

684

## 685 8. References

686

687 Abbott, P.M., Davies, S.M., 2012. Volcanism and the Greenland ice-cores: The tephra record.  
688 Earth-Science Reviews 115, 173-191.

689 Blockley, S.P., Bourne, A.J., Brauer, A., Davies, S.M., Hardiman, M., Harding, P.R., Lane, C.S.,  
690 MacLeod, A., Matthews, I.P., Pyne-O'Donnell, S.D., 2014. Tephrochronology and the  
691 extended intimate (integration of ice-core, marine and terrestrial records) event  
692 stratigraphy 8–128 ka b2k. Quaternary Science Reviews 106, 88-100.

693 Blockley, S.P.E., Pyne-O'Donnell, S.D.F., Lowe, J.J., Matthews, I.P., Stone, A., Pollard, A.M.,  
694 Turney, C.S.M., Molyneux, E.G., 2005. A new and less destructive laboratory procedure for  
695 the physical separation of distal glass tephra shards from sediments. Quaternary Science  
696 Reviews 24, 1952-1960.

697 Blockley, S.P.E., Lane, C.S., Hardiman, M., Rasmussen, S.O., Seierstad, I.K., Steffensen, J.P.,  
698 Svensson, A., Lotter, A.F., Turney, C.S.M., Bronk Ramsey, C., 2012. Synchronisation of  
699 palaeoenvironmental records over the last 60,000 years, and an extended INTIMATE 1 event  
700 stratigraphy to 48,000 b2k. Quaternary Science Reviews 36, 2-10.

701 Brauer, A., Endres, C., Negendank, J.F.W., 1999. Lateglacial calendar year chronology based  
702 on annually laminated sediments from Lake Meerfelder Maar, Germany. Quaternary  
703 International 61, 17-25.

- 704 Brauer, A., Endres, C., Zolitschka, B., Negendank, J.F.W., 2000a. AMS radiocarbon and varve  
705 chronology from the annually laminated sediment record of Lake Meerfelder Maar,  
706 Germany. *Radiocarbon* 42, 355-368.
- 707 Brauer, A., Günter, C., Johnsen, S.J., Negendank, J.F.W., 2000b. Land-ice teleconnections of  
708 cold climatic periods during the last Glacial/Interglacial transition. *Climate Dynamics* 16,  
709 229-239.
- 710 Brauer, A., Allen, J.R.M., Mingram, J., Dulski, P., Wulf, S., Huntley, B., 2007. Evidence for last  
711 interglacial chronology and environmental change from Southern Europe. *Proceedings of*  
712 *the National Academy of Sciences of the United States of America* 104, 450-455.
- 713 Brauer, A., Haug, G.H., Dulski, P., Sigman, D.M., Negendank, J.F.W., 2008. An abrupt wind  
714 shift in western Europe at the onset of the Younger Dryas cold period. *Nature Geoscience* 1,  
715 520-523.
- 716 Brauer, A., Hajdas, I., Blockley, S.P., Ramsey, C.B., Christl, M., Ivy-Ochs, S., Moseley, G.E.,  
717 Nowaczyk, N.N., Rasmussen, S.O., Roberts, H.M., 2014. The importance of independent  
718 chronology in integrating records of past climate change for the 60–8 ka INTIMATE time  
719 interval. *Quaternary Science Reviews* 106, 47-66.
- 720 Bronk Ramsey, C., 2001. Development of the Radiocarbon Program OxCal. *Radiocarbon* 43,  
721 355-364.
- 722 Bronk Ramsey, C., Albert, P.G., Blockley, S.P., Hardiman, M., Housley, R.A., Lane, C.S., Lee, S.,  
723 Matthews, I.P., Smith, V.C., Lowe, J., in press-a. Improved age estimates for key Late  
724 Quaternary European tephra horizons in the RESET lattice. *Quaternary Science Reviews*.
- 725 Bronk Ramsey, C., Housley, R.A., Lane, C.S., Smith, V.C., Pollard, A.M., in press-b. The RESET  
726 tephra database and associated analytical tools. *Quaternary Science Reviews*.
- 727 Büchel, G., Lorenz, V., 1984. Zum Alter des Meerfelder Maars. G. Irion & JFW Negendank,  
728 *Cour. Forsch. Inst. Senckenberg* 65, 13-15.
- 729 Chambers, F.M., Daniell, J.R.G., Hunt, J.B., Molloy, K., O'Connell, M., 2004.  
730 Tephrostratigraphy of An Loch Mór, Inis Oírr, western Ireland: Implications for Holocene  
731 tephrochronology in the northeastern Atlantic region. *Holocene* 14, 703-720.
- 732 Civetta, L., Cornette, Y., Crisci, P.Y., Orsi, G., Requejo, C.S., 1984. Geology, geochronology  
733 and chemical evolution of the island of Pantelleria. *Geological Magazine* 121, 541-562.
- 734 Davies, S.M., Abbott, P.M., Pearce, N.J.G., Wastegård, S., Blockley, S.P.E., 2012. Integrating  
735 the INTIMATE records using tephrochronology: Rising to the challenge. *Quaternary Science*  
736 *Reviews* 36, 11-27.

- 737 Deino, A.L., Orsi, G., de Vita, S., Piochi, M., 2004. The age of the Neapolitan Yellow Tuff  
738 caldera-forming eruption (Campi Flegrei caldera - Italy) assessed by  $^{40}\text{Ar}/^{39}\text{Ar}$  dating  
739 method. *Journal of Volcanology and Geothermal Research* 133, 157-170.
- 740 Dugmore, A.J., Larsen, G., Newton, A.J., 1995. Seven tephra isochrones in Scotland.  
741 *Holocene* 5, 257-266.
- 742 Gertisser, R., Self, S., Gaspar, J.L., Kelley, S.P., Pimentel, A., Eikenberg, J., Barry, T.L.,  
743 Pacheco, J.M., Queiroz, G., Vespa, M., 2010. Ignimbrite stratigraphy and chronology on  
744 Terceira Island, Azores.
- 745 Hajdas, I., 1993. AMS radiocarbon dating and varve chronology of Lake Soppensee: 6000 to  
746 12 000  $^{14}\text{C}$  years BP. *Climate Dynamics* 9, 107-116.
- 747 Housley, R.A., Lane, C.S., Cullen, V.L., Weber, M.J., Riede, F., Gamble, C.S., Brock, F., 2012.  
748 Icelandic volcanic ash from the Late-glacial open-air archaeological site of Ahrenshöft LA 58  
749 D, North Germany. *Journal of Archaeological Science* 39, 708-716.
- 750 Jochum, K.P., Nohl, U., Herwig, K., Lammel, E., Stoll, B., Hofmann, A.W., 2005. GeoReM: A  
751 new geochemical database for reference materials and isotopic standards. *Geostandards  
752 and Geoanalytical Research* 29, 333-338.
- 753 Jochum, K.P., Stoll, B., Herwig, K., Willbold, M., Hofmann, A.W., Amini, M., Aarburg, S.,  
754 Abouchami, W., Hellebrand, E., Mocek, B., Raczek, I., Stracke, A., Alard, O., Bouman, C.,  
755 Becker, S., Dücking, M., Bratz, H., Klemd, R., de Bruin, D., Canil, D., Cornell, D., de Hoog, C.J.,  
756 Dalpe, C., Danyushevsky, L., Eisenhauer, A., Gao, Y.J., Snow, J.E., Goschopf, N., Gunther, D.,  
757 Latkoczy, C., Guillong, M., Hauri, E.H., Hofer, H.E., Lahaye, Y., Horz, K., Jacob, D.E.,  
758 Kassemann, S.A., Kent, A.J.R., Ludwig, T., Zack, T., Mason, P.R.D., Meixner, A., Rosner, M.,  
759 Misawa, K.J., Nash, B.P., Pfander, J., Premo, W.R., Sun, W.D.D., Tiepolo, M., Vannucci, R.,  
760 Vennemann, T., Wayne, D., Woodhead, J.D., 2006. MPI-DING reference glasses for in situ  
761 microanalysis: new reference values for element concentrations and isotope ratios.  
762 *Geochemistry Geophysics Geosystems* 7.
- 763 Johannesson, H.L., E. M.; Wastegård, S., in press. Proximal tephra glass geochemistry from  
764 eruptions in the Azores archipelago and links with distal sites in Ireland. *The Holocene*.
- 765 Koren, J.H., Svendsen, J.I., Mangerud, J., Furnes, H., 2008. The Dimna Ash - a 12.8  $^{14}\text{C}$  ka-old  
766 volcanic ash in Western Norway. *Quaternary Science Reviews* 27, 85-94.
- 767 Lacasse, C., Garbe-Schönberg, C.D., 2001. Explosive silicic volcanism in Iceland and the Jan  
768 Mayen area during the last 6Ma: sources and timing of major eruptions. *Journal of  
769 Volcanology and Geothermal Research* 107, 113-147.
- 770 Lane, C.S., Andrič, M., Cullen, V.L., Blockley, S.P.E., 2011a. The occurrence of distal Icelandic  
771 and Italian tephra in the Lateglacial of Lake Bled, Slovenia. *Quaternary Science Reviews* 30,  
772 1013-1018.

- 773 Lane, C.S., Blockley, S.P.E., Bronk Ramsey, C., Lotter, A.F., 2011b. Tephrochronology and  
774 absolute centennial scale synchronisation of European and Greenland records for the last  
775 glacial to interglacial transition: A case study of Soppensee and NGRIP. *Quaternary*  
776 *International*, 145-156.
- 777 Lane, C.S., Blockley, S.P.E., Lotter, A.F., Finsinger, W., Filippi, M.L., Matthews, I.P., 2012a. A  
778 regional tephrostratigraphic framework for central and southern European climate archives  
779 during the Last Glacial to Interglacial transition: Comparisons north and south of the Alps.  
780 *Quaternary Science Reviews* 36, 50-58.
- 781 Lane, C.S., Blockley, S.P.E., Mangerud, J., Smith, V.C., Lohne, Ø., Tomlinson, E.L., Matthews,  
782 I.P., Lotter, A.F., 2012b. Was the 12.1ka Icelandic Vedde Ash one of a kind? *Quaternary*  
783 *Science Reviews* 33, 87-99.
- 784 Lane, C.S., De Klerk, P., Cullen, V.L., 2012c. A tephrochronology for the Lateglacial  
785 palynological record of the Endinger Bruch (Vorpommern, north-east Germany). *Journal of*  
786 *Quaternary Science* 27, 141-149.
- 787 Lane, C.S., Brauer, A., Blockley, S.P.E., Dulski, P., 2013. Volcanic ash reveals time-  
788 transgressive abrupt climate change during the Younger Dryas. *Geology* 41, 1251-1254.
- 789 Lane, C.S., Cullen, V., White, D., Bramham-Law, C., Smith, V., 2014. Cryptotephra as a dating  
790 and correlation tool in archaeology. *Journal of Archaeological Science* 42, 42-50.
- 791 Le Bas, M.J., Le Maitre, R.W., Streckeisen, A., Zanettin, B., 1986. A chemical classification of  
792 volcanic rocks based on the total alkali-silica diagram. *Journal of Petrology* 27, 745-750.
- 793 Litt, T., Stebich, M., 1999. Bio- and chronostratigraphy of the lateglacial in the Eifel region,  
794 Germany. *Quaternary International* 61, 5-16.
- 795 Lohne, Ø.S., Mangerud, J.A.N., Birks, H.H., 2013. Precise  $^{14}\text{C}$  ages of the Vedde and  
796 Saksunarvatn ashes and the Younger Dryas boundaries from western Norway and their  
797 comparison with the Greenland Ice Core (GISCC05) chronology. *Journal of Quaternary*  
798 *Science* 28, 490-500.
- 799 Lowe, J.J., 2001. Abrupt climatic changes in Europe during the last glacial-interglacial  
800 transition: The potential for testing hypotheses on the synchronicity of climatic events using  
801 tephrochronology. *Global and Planetary Change* 30, 73-84.
- 802 Macdonald, R., 1974. Nomenclature and petrochemistry of the peralkaline oversaturated  
803 extrusive rocks. *Bulletin Volcanologique* 38, 498-516.
- 804 Magny, M., Vannièrè, B., Calò, C., Millet, L., Leroux, A., Peyron, O., Zanchetta, G., La Mantia,  
805 T., Tinner, W., 2011. Holocene hydrological changes in south-western Mediterranean as  
806 recorded by lake-level fluctuations at Lago Preola, a coastal lake in southern Sicily, Italy.  
807 *Quaternary Science Reviews* 30, 2459-2475.

- 808 Mahood, G.A., Hildreth, W., 1986. Geology of the peralkaline volcano at Pantelleria, Strait of  
809 Sicily. *Bulletin of Volcanology* 48, 143-172.
- 810 Mangerud, J., Lie, S.E., Furnes, H., Kristiansen, I.L., Lømo, L., 1984. A Younger Dryas Ash Bed  
811 in western Norway, and its possible correlations with tephra in cores from the Norwegian  
812 Sea and the North Atlantic. *Quaternary Research* 21, 85-104.
- 813 Martin-Puertas, C., Brauer, A., Dulski, P., Brademann, B., 2012a. Testing climate-proxy  
814 stationarity throughout the Holocene: an example from the varved sediments of Lake  
815 Meerfelder Maar (Germany). *Quaternary Science Reviews* 58, 56-65.
- 816 Martin-Puertas, C., Matthes, K., Brauer, A., Muscheler, R., Hansen, F., Petrick, C., Aldahan,  
817 A., Possnert, G., van Geel, B., 2012b. Regional atmospheric circulation shifts induced by a  
818 grand solar minimum. *Nature Geosci* 5, 397-401.
- 819 Matthews, I.P., Birks, H.H., Bourne, A.J., Brooks, S.J., Lowe, J.J., Macleod, A., Pyne-O'Donnell,  
820 S.D.F., 2011. New age estimates and climatostratigraphic correlations for the borrobol and  
821 penifiler tephtras: Evidence from Abernethy Forest, Scotland. *Journal of Quaternary Science*  
822 26, 247-252.
- 823 Mortensen, A.K., Bigler, M., Grönvold, K., Steffensen, J.P., Johnsen, S.J., 2005. Volcanic ash  
824 layers from the last glacial termination in the NGRIP ice core. *Journal of Quaternary Science*  
825 20, 209-219.
- 826 Muscheler, R., Kromer, B., Björck, S., Svensson, A., Friedrich, M., Kaiser, K., Southon, J.,  
827 2008. Tree rings and ice cores reveal 14C calibration uncertainties during the Younger Dryas.  
828 *Nature Geoscience* 1, 263-267.
- 829 Plunkett, G., 2009. Land-use patterns and cultural change in the Middle to Late Bronze Age  
830 in Ireland: Inferences from pollen records. *Vegetation History and Archaeobotany* 18, 273-  
831 295.
- 832 Rach, O., Brauer, A., Wilkes, H., Sachse, D., 2014. Delayed hydrological response to  
833 Greenland cooling at the onset of the Younger Dryas in western Europe. *Nature Geoscience*  
834 7, 109-112.
- 835 Rasmussen, S.O., Andersen, K.K., Svensson, A.M., Steffensen, J.P., Vinther, B.M., Clausen,  
836 H.B., Siggaard-Andersen, M.L., Johnsen, S.J., Larsen, L.B., Dahl-Jensen, D., Bigler, M.,  
837 Röthlisberger, R., Fischer, H., Goto-Azuma, K., Hansson, M.E., Ruth, U., 2006. A new  
838 Greenland ice core chronology for the last glacial termination. *Journal of Geophysical*  
839 *Research D: Atmospheres* 111, D06102.
- 840 Reilly, E., Mitchell, F.J., 2014. Establishing chronologies for woodland small hollow and mor  
841 humus deposits using tephrochronology and radiocarbon dating. *The Holocene*.

- 842 Reimer, P.J., Bard, E., Bayliss, A., Beck, J.W., Blackwell, P.G., Ramsey, C.B., Buck, C.E., Cheng,  
843 H., Edwards, R.L., Friedrich, M., 2013. IntCal13 and Marine13 radiocarbon age calibration  
844 curves 0–50,000 years cal BP. *Radiocarbon* 55, 1869-1887.
- 845 Riede, F., Bazely, O., Newton, A.J., Lane, C.S., 2011. A Laacher See-eruption supplement to  
846 Tephabase: Investigating distal tephra fallout dynamics. *Quaternary International* 246, 134-  
847 144.
- 848 Schmidt, R., Van Den Bogaard, C., Merkt, J., Müller, J., 2002. A new Lateglacial  
849 chronostratigraphic tephra marker for the south-eastern Alps: The Neapolitan Yellow Tuff  
850 (NYT) in Längsee (Austria) in the context of a regional biostratigraphy and palaeoclimate.  
851 *Quaternary International* 88, 45-56.
- 852 Siani, G., Sulpizio, R., Paterne, M., Sbrana, A., 2004. Tephrostratigraphy study for the last  
853 18,000 14C years in a deep-sea sediment sequence for the South Adriatic. *Quaternary  
854 Science Reviews* 23, 2485-2500.
- 855 Smith, V.C., Isaia, R., Pearce, N.J.G., 2011. Tephrostratigraphy and glass compositions of  
856 post-15 kyr Campi Flegrei eruptions: Implications for eruption history and  
857 chronostratigraphic markers. *Quaternary Science Reviews* 30, 3638-3660.
- 858 Steffensen, J.P., Andersen, K.K., Bigler, M., Clausen, H.B., Dahl-Jensen, D., Fischer, H., Goto-  
859 Azuma, K., Hansson, M., Johnsen, S.J., Jouzel, J., Masson-Delmotte, V., Popp, T., Rasmussen,  
860 S.O., Röthlisberger, R., Ruth, U., Stauffer, B., Siggaard-Andersen, M.L., Sveinbjörnsdóttir,  
861 Á.E., Svensson, A., White, J.W.C., 2008. High-resolution greenland ice core data show abrupt  
862 climate change happens in few years. *Science* 321, 680-684.
- 863 Tomlinson, E.L., Thordarson, T., Müller, W., Thirlwall, M., Menzies, M.A., 2010.  
864 Microanalysis of tephra by LA-ICP-MS - Strategies, advantages and limitations assessed using  
865 the Thorsmörk ignimbrite (Southern Iceland). *Chemical Geology* 279, 73-89.
- 866 Tomlinson, E.L., Arienzo, I., Civetta, L., Wulf, S., Smith, V.C., Hardiman, M., Lane, C.S.,  
867 Carandente, A., Orsi, G., Rosi, M., Müller, W., Menzies, M.A., 2012. Geochemistry of the  
868 Phlegraean Fields (Italy) proximal sources for major Mediterranean tephras: Implications for  
869 the dispersal of Plinian and co-ignimbritic components of explosive eruptions. *Geochimica et  
870 Cosmochimica Acta* 93, 102-108.
- 871 Tomlinson, E.L., Smith, V.C., Albert, P.G., Aydar, E., Civetta, L., Cioni, R., Çubukçu, E.,  
872 Gertisser, R., Isaia, R., Menzies, M.A., Orsi, G., Rosi, M., Zanchetta, G., in press. The major  
873 and trace element glass compositions of the productive Mediterranean volcanic sources:  
874 tools for correlating distal tephra layers in and around Europe. *Quaternary Science Reviews*.
- 875 Turney, C.S.M., 1998. Extraction of rhyolitic component of Vedde microtephra from  
876 minerogenic lake sediments. *Journal of Paleolimnology* 19, 199.

- 877 van den Bogaard, P., Schmincke, H.U., 1985. Laacher See tephra: a widespread isochronous  
878 late Quaternary tephra layer in central and northern Europe. *Geological Society of America*  
879 *Bulletin* 96, 1554-1571.
- 880 van Geel, B., Engels, S., Martin-Puertas, C., Brauer, A., 2013. Ascospores of the parasitic  
881 fungus *Kretzschmaria deusta* as rainstorm indicators during a late Holocene beech-forest  
882 phase around lake Meerfelder Maar, Germany. *Journal of Paleolimnology* 50, 33-40.
- 883 Wastegård, S., 2002. Early to middle Holocene silicic tephra horizons from the Katla volcanic  
884 system, Iceland: New results from the Faroe Islands. *Journal of Quaternary Science* 17, 723-  
885 730.
- 886 Wulf, S., Kraml, M., Brauer, A., Keller, J., Negendank, J.F.W., 2004. Tephrochronology of the  
887 100ka lacustrine sediment record of Lago Grande di Monticchio (southern Italy). *Quaternary*  
888 *International* 122, 7-30.
- 889 Wulf, S., Kraml, M., Keller, J., 2008. Towards a detailed distal tephrostratigraphy in the  
890 Central Mediterranean: The last 20,000 yrs record of Lago Grande di Monticchio. *Journal of*  
891 *Volcanology and Geothermal Research* 177, 118-132.
- 892 Wulf, S., Keller, J., Paterne, M., Mingram, J., Lauterbach, S., Opitz, S., Sottili, G., Giaccio, B.,  
893 Albert, P.G., Satow, C., Tomlinson, E.L., Viccaro, M., Brauer, A., 2012. The 100-133 ka record  
894 of Italian explosive volcanism and revised tephrochronology of Lago Grande di Monticchio.  
895 *Quaternary Science Reviews* 58, 104-123.
- 896 Wulf, S., Ott, F., Słowiński, M., Noryśkiewicz, A.M., Dräger, N., Martin-Puertas, C., Czymzik,  
897 M., Neugebauer, I., Dulski, P., Bourne, A.J., Błaszczewicz, M., Brauer, A., 2013. Tracing the  
898 Laacher See Tephra in the varved sediment record of the Trzechowskie palaeolake in central  
899 Northern Poland. *Quaternary Science Reviews* 76, 129-139.
- 900 Zolitschka, B., Negendank, J.F.W., Lottermoser, B.G., 1995. Sedimentological proof and  
901 dating of the Early Holocene volcanic eruption of Ulmener Maar (Vulkaneifel, Germany).  
902 *Geologische Rundschau* 84, 213-219.
- 903 Zöller, L., Blanchard, H., 2009. The partial heat–longest plateau technique: Testing TL dating  
904 of Middle and Upper Quaternary volcanic eruptions in the Eifel Area, Germany. *E&G*  
905 *Quaternary Science Journal* 58, 86-106.